A TPC for sPHENIX

TK Hemmick

Topics to touch upon.

- Physics Performance:
  - Capability.
  - Performance Spec.
- Next Generation TPC Concepts:
  - Overview of Gate-less TPC Concepts.
  - Space Charge.
  - Aces in the hole.
- R&D Achievements/Capabilities.
- Progress on field cage concept and construction.

Momentum Resolution-I

Position Resolution:
(Silicon best)

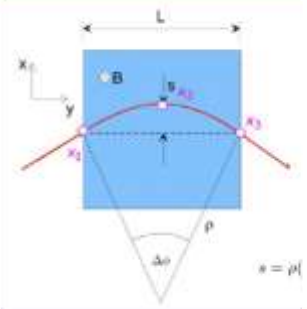

$$s = \rho(1 - \cos\frac{\Delta\phi}{2}) \approx \rho(1 - (1 - \frac{1}{2}\frac{\Delta\phi^2}{4})) = \rho\frac{\Delta\phi^2}{2} \approx \frac{0.3}{8}\frac{L^2 B}{p_T}$$

$$\frac{\sigma_{p_T}}{p_T} = \frac{\sigma_s}{s} = \frac{8\sigma_s}{0.3L^2B}p_T$$

$$\frac{\sigma_{p_T}}{p_T} = \sqrt{\frac{720}{(N+4)}}\frac{\sigma_x}{0.3L^2B}p_T$$

Multiple Scattering:
(Hybrid better)

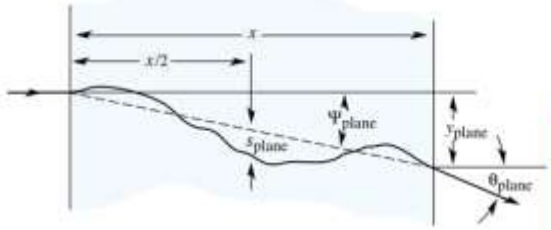

$$\phi_0 = \frac{13.6\text{MeV}}{\beta c p_T} z\sqrt{\frac{L}{X_0}}\,[1 + 0.038\ln\frac{L}{X_0}]$$

$$\frac{\sigma^{ms}_{p_T}}{p_T} = \frac{0.052}{\beta BL}\sqrt{\frac{L}{X_0}}[1 + 0.038\ln\frac{L}{X_0})].$$

3 Dimensions:

$$\frac{\sigma_p}{p} = \sqrt{\left(\frac{\sigma_{ms}}{\sqrt{\sin\theta}}\right)^2 + \left(\sigma_{det}\; p\sin\theta\right)^2 + \left(\sigma^{det}_{\theta}\;\cot\theta\sin\theta\right)^2 + \left(\frac{\sigma^{ms}_{\theta}}{\sqrt{\sin_\theta}}\frac{\cot\theta}{p}\right)^2}$$

Bremsstrahlung:
(Hybrid better)

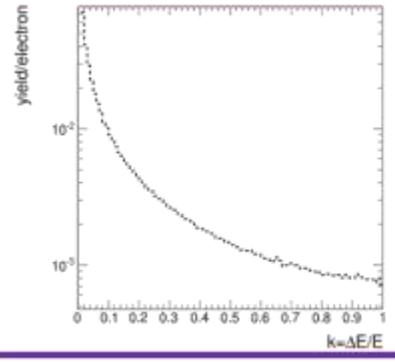

$$k \equiv \frac{\Delta E}{E} \qquad \frac{d\sigma}{dk} = \frac{A}{X_0 N_A k}\left(\frac{4}{3} - \frac{4}{3}k + k^2\right)$$

$$N_\gamma = \frac{L}{X_0}\left(\frac{4}{3}\;\ln\frac{k_{max}}{k_{min}} - \frac{4(k_{max} - k_{min})}{3} + \frac{k^2_{max} - k^2_{min}}{2}\right)$$

Momentum Resolution calculated for all options from analytic and full Monte Carlo Simulations

Momentum Resolution-II

Station	Layer	radius (cm)	pitch (μm)	sensor length (cm)	depth (μm)	total thickness X_0%	area (m^2)
Pixel	1	2.4	50	0.425	200	1.3	0.034
Pixel	2	4.4	50	0.425	200	1.3	0.059
S0a	3	7.5	58	9.6	240	1.0	0.18
S0b	4	8.5	58	9.6	240	1.0	0.18
S1a	5	31.0	58	9.6	240	0.6	1.4
S1b	6	34.0	58	9.6	240	0.6	1.4
S2	7	64.0	60	9.6	320	1.0	6.5

layer	radius (cm)	total thickness % X_0	$\Delta L/L$	c_{ms} (mrad)	σ_{ms} (mrad)
VTX 1	2.7	1.3	0.95	1.8	1.7
VTX 2	4.6	1.3	0.92	1.8	1.7
air	15	0.1	0.73	0.03	0.02
field cage	30	1.0	0.45	1.12	0.5

- Analytic and full Geant simulations performed.
- All results agree remarkably well.
- All options meet the experiment design goal.

Reference Design

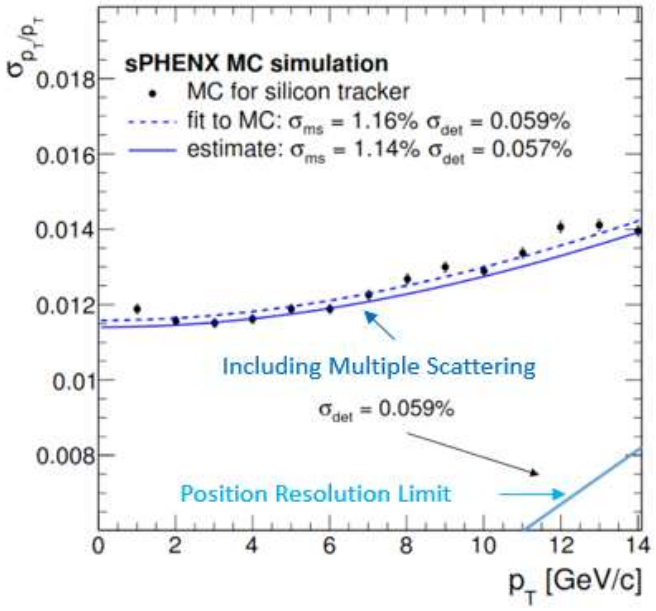

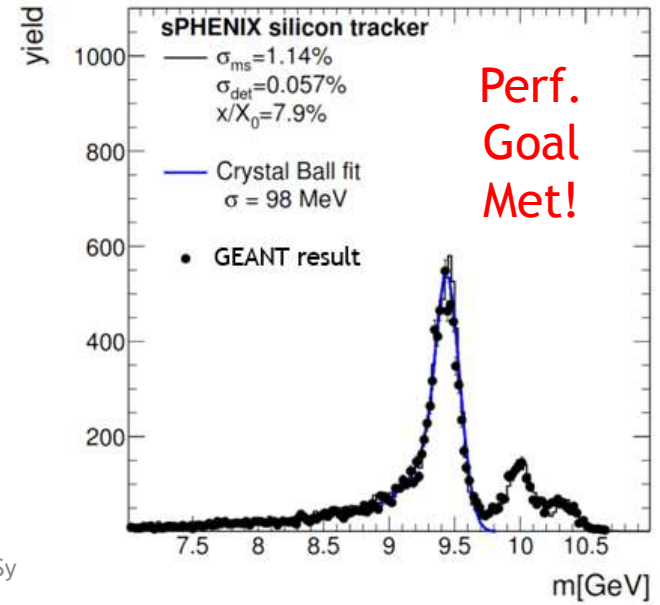

Hybrid: Reuse Pixels + TPC

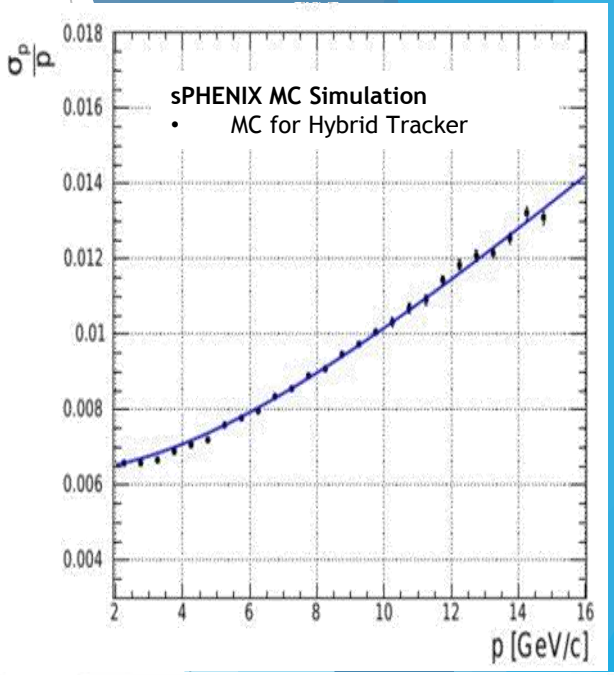

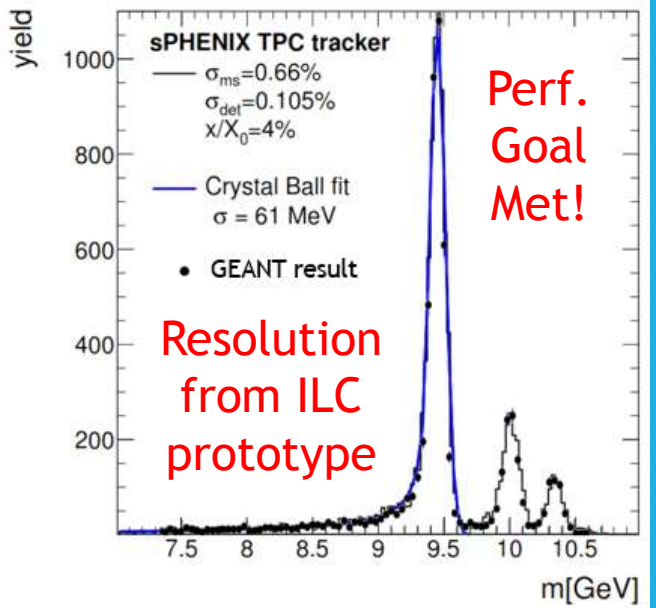

Design Drivers

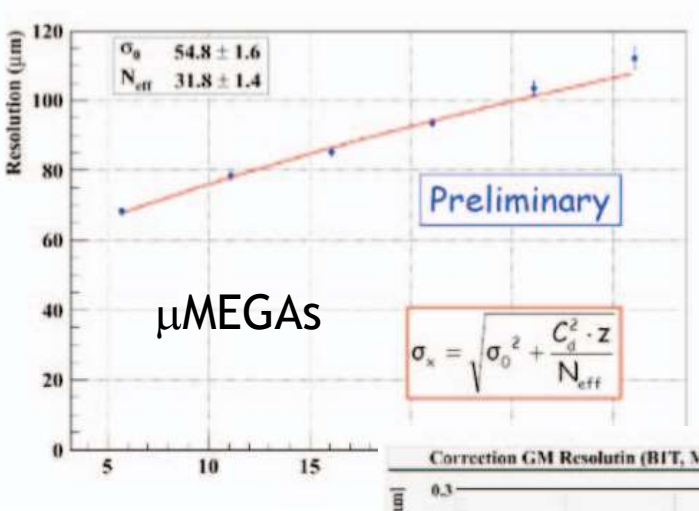

Does not include space charge considerations,

Significant at high rate.

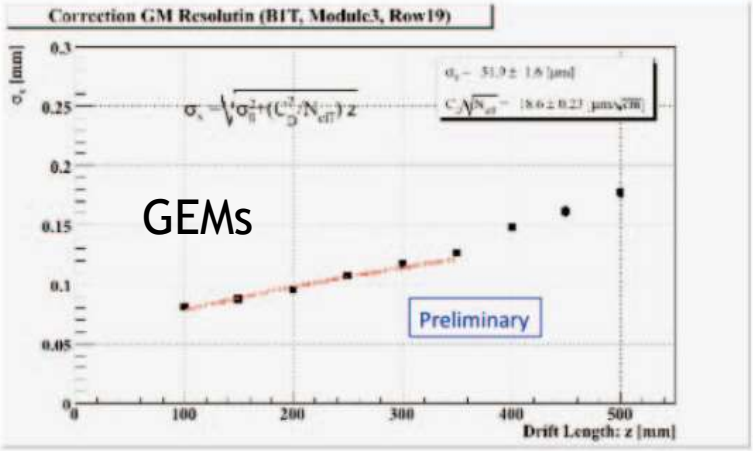

- ILC R&D results very encouraging.
- ILC R&D results were used as the basis of the simulations presented previously.
  - ILC ~ 150 μm after 2.5 meters drift.
  - sPHENIX requirement 250 μm after 80 cm drift.

Hybrid Tracker Option

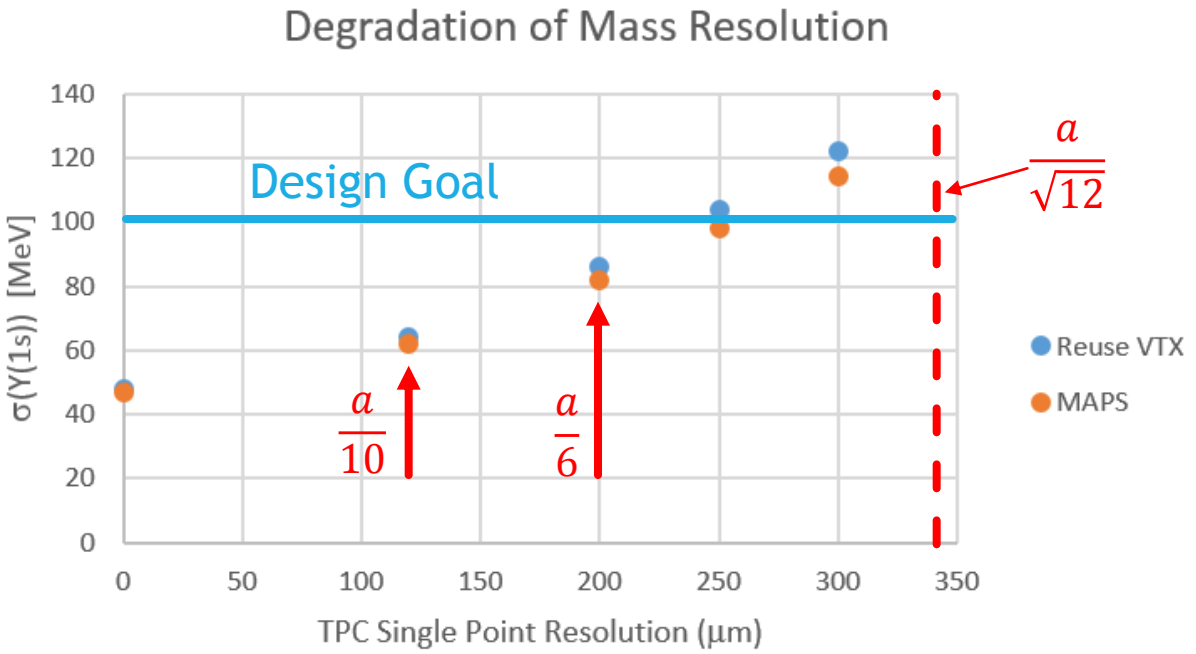

- The Upsilon mass width for the hybrid setup is influenced by the single point resolution.
- Current calculations assume an RMS resolution of 1/10 the pad size ($\frac{a}{10}$).
- The hybrid system will meet the mass resolution goal with an RMS position resolution of 250 μm.

Considerations for ALICE TPC Upgrade:

- Run 3 @ CERN: 50 kHz Pb-Pb collisions.
- Gated TPC (current device) uncompetitive in high rate environments.
- Un-gated TPC (new technology) allows for continuous readout device by using Micro-Pattern Gas Detectors (MPGD) to reduce ion back flow to below 1% at a gain of 2000X.
  - Ion Back Flow (100% for wire chamber gain) leads to position distortion in TPC due to "space charge" effects.
  - Normal TPC:
    - Fast detectors detect event.
    - Drift electron gate opens (t=drift time), drift gate closes (t=positive ion absorption time)
- MPGD are being used by all CERN Experiments during upgrade:
  - ATLAS muon detectors using micro-MEGA layers (1m x 2m)…{Polychronakos @ BNL}
  - CMS muon detector upgrade using large area GEM-based detectors.

But a TPC is "slow"

- New concept in DAQ readout.
- TPC is a continuous source of processed (baseline restoration, zero suppression) data that intrinsically knows "when" it occurred.
- All time intervals contain multiple events that are distinguished by pointing to apparently displaced vertices.
- "Events" involve the fast detectors referencing the appropriate time interval of the continual TPC data.
- NOTE: Significant consequences for online/offline architecture.
- New "figure of merit" is the mean number of events present during a single drift period and results in a compromise condition on gas speed.
  - Slow gas = higher mean number of events.
  - Slow gas = particle pair separation smaller (harder to distinguish close tracks)

Existing ALICE simulations provide an interesting benchmark point for us

Why MPGD?

- In the MPGD structure, "routing" of charge through microscopic structures (electrons for primary gain; ions for backflow) effectively amplifies the difference in transport properties of ions and electrons.
- The result is that ions land on the physical structures (mesh of microMEGA; foil for GEM) with higher probability than electrons.
- Therefore, gain can be achieved (electron transport) with low ion back flow (ion transport).

μMEGA are best for ion feedback. Concerns about sparking.

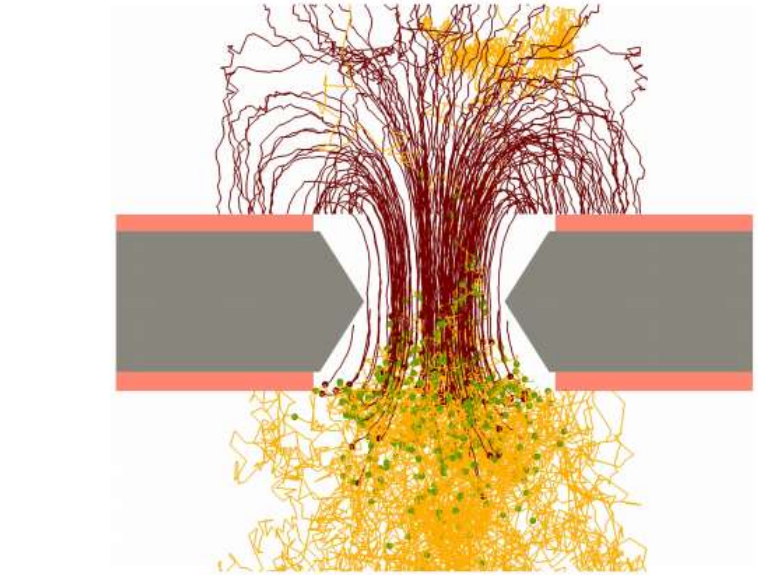

Figure 4.2: Garfield / Magboltz simulation of charge dynamics for electrons (two in this simulation) entering into a GEM hole [4]. Electron drift paths are shown as light lines, ion drift paths as dark lines. Dots mark places where ionization (multiplication) processes have occurred. The paths have been projected onto the cross section plane.

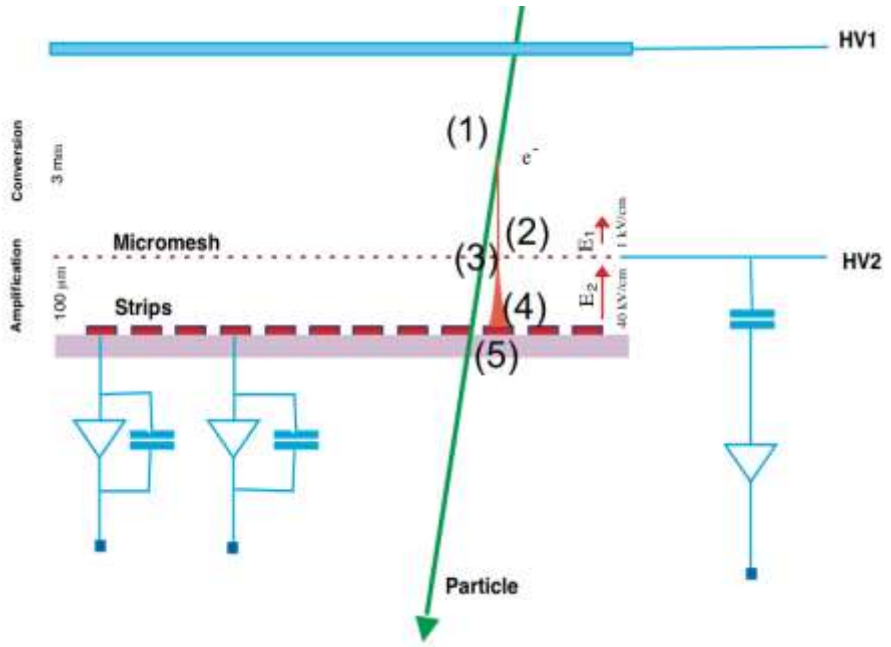

"Staggered" Draft Field

NOTE: Unavoidable feedback 1st GEM

- Electron/Ion drift differences "enhanced" by staggered drift field options.
- Leads to four layers of GEM.
- Other considerations:
  - Hole pattern rotation.
  - Hole spacing changes.

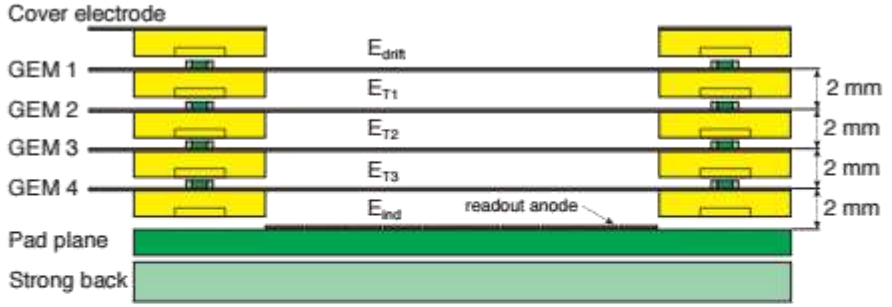

Figure 4.6: Schematic exploded cross section of the GEM stack. Each GEM foil is glued onto a 2 mm thick support frame defining the gap. The designations of the GEM foils and electric fields used in this TDR are also given. E_{drift} corresponds to the drift field, E_{Ti} denote the transfer fields between GEM foils, and E_{ind} the induction field between the fourth GEM and the pad plane. The readout anode (see Eq. (4.2)) is indicated as well. The drift cathode is defined by the drift electrode not shown on this schematic.

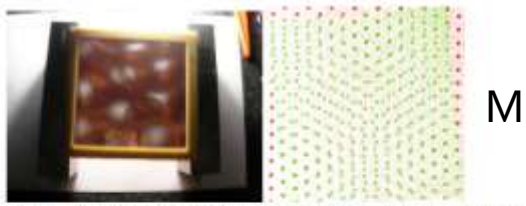

Moire

Uniform

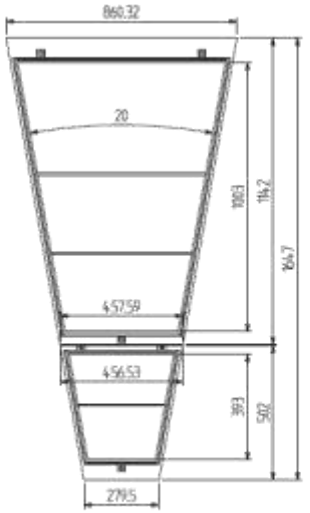

40 cm

Figure 4.4 shows an exploded view of a GEM IROC. It consists of the following components:

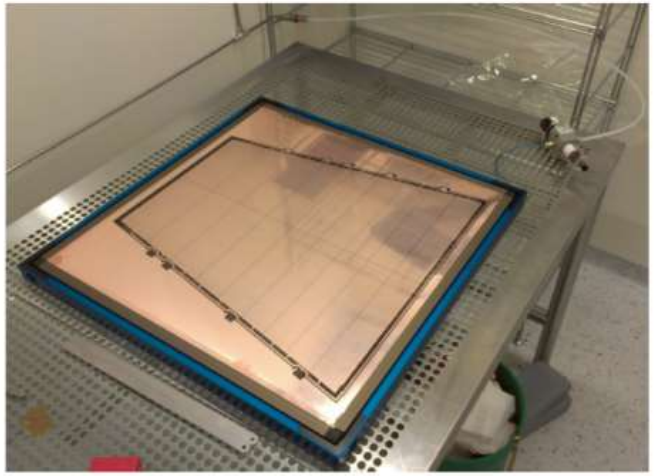

Figure 4.7: Photograph of an IROC GEM foil in the stretching frame.

Measuring Ion Back Flow

- Using new HV modules (cascaded HV power supply) one can measure all currents on all layers and learn backflow.
- Fundamental limit:
  - 1st GEM ions are 100% coupled into the TPC.
  - Best IBF when 1st layer is low gain.
  - CAVEAT!
    - For *any* multi-stage avalanche, 1st stage gain provides limit on eventual energy resolution.
    - Good dE/dx from LARGE gain in the first GEM.
  - All concepts will exhibit competing behavior of dE/dx resolution vs IBF.

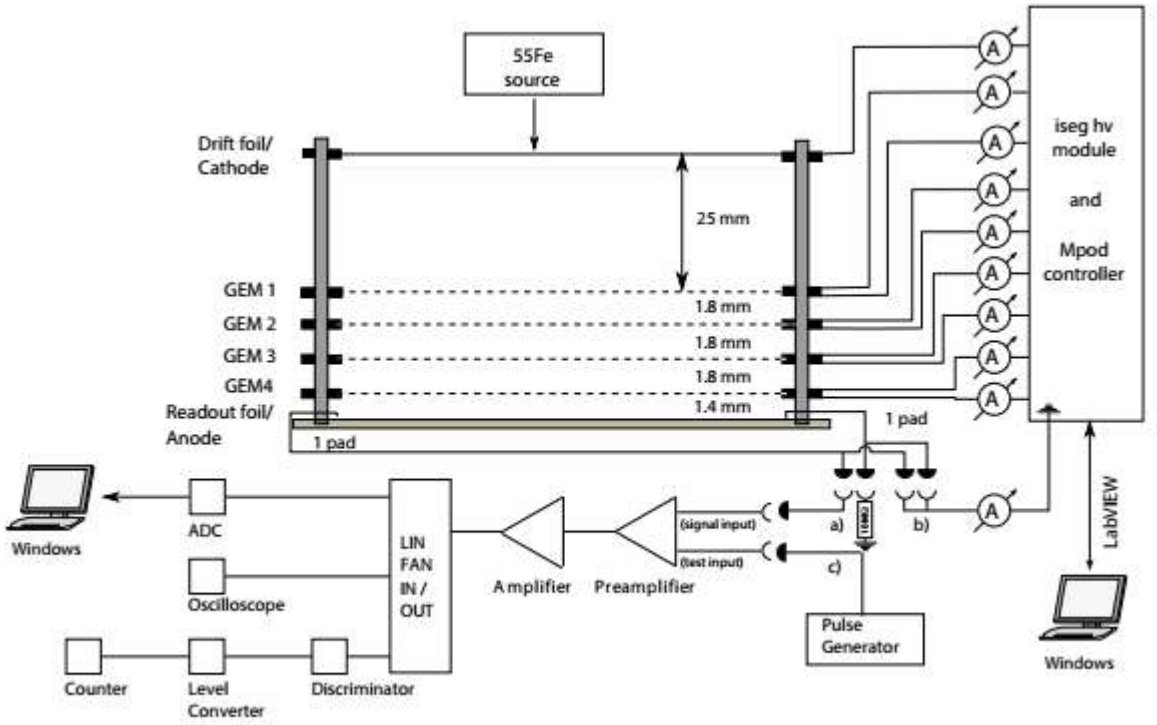

Figure 5.1: Sketch of the Munich quadruple GEM setup.

Bench Measurements

- Design specs:
  - IBF < 1% at gain=2000X
  - Resolution $\left(\frac{\sigma}{\langle E \rangle}(^{55}Fe)\right) < 12\%$
- Banana curves result principally from adjusting the 1st GEM gain.
- Other tricks (e.g. hole spacing…) help as well.
- NOTE: In the end there are four GEM designs (one per layer); each differing in hole pattern.
- Production requires staggered use of CERN shops with different masks in order to match chamber production schedule.

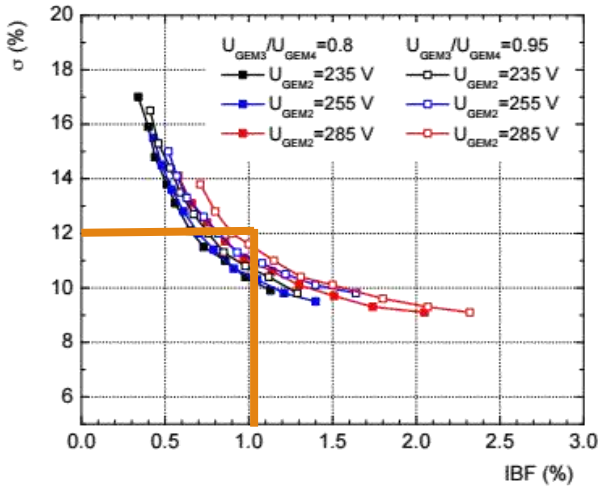

Figure 5.4: Correlation between ion backflow and energy resolution at 5.9 keV in a quadruple S-LP-LP-S GEM in Ne-CO_2-N_2 (90-10-5) for various settings of ΔU_{GEM2}. The voltage on GEM 1 increases for a given setting between 225 and 315 V from left to right. The voltages on GEM 3 and GEM 4 are adjusted to achieve a total effective gain of 2000, while keeping their ratio fixed. The transfer and induction fields are 4, 2, 0.1 and 4 kV/cm, respectively.

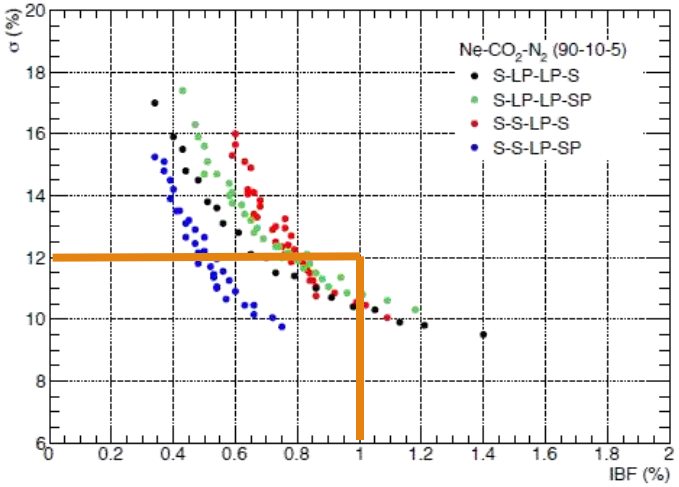

Figure 3.10: Correlation between energy resolution and ion backflow in various quadruple GEM systems in Ne-CO_2-N_2 (90-10-5), occuring by variation of ΔU_{GEM1} and ΔU_{GEM2}. All transfer fields are optimized in foregoing scans, respectively. The gain was adjusted to 2000 by fine tuning of ΔU_{GEM3} and ΔU_{GEM4}, while keeping $\Delta U_{GEM3}/\Delta U_{GEM4} = 0.8$.

Effects of Space Charge on TPC performance

- The process of measuring trajectories can be factorized:
  - Position resolution of hits on a pad plane (easy part).
  - Extrapolating back through the gas volume (hard part).
- Next generation TPCs feature high rate but suffer from space charge distortions that complicate the extrapolation from the measured coordinate back to the source point.
- Positive ion space charge effectively “pulls” the electron trajectories toward the center of the TPC.
- The magnitude of the distortion can be very large:
  - STAR ~10 cm.
  - ALICE 10-20 cm.
- The average deflection can be determined by measurement and calibration to high precision.
- Final device performance is limited by the FLUCTUATIONS in the deflection (i.e. percentages of the deflection).

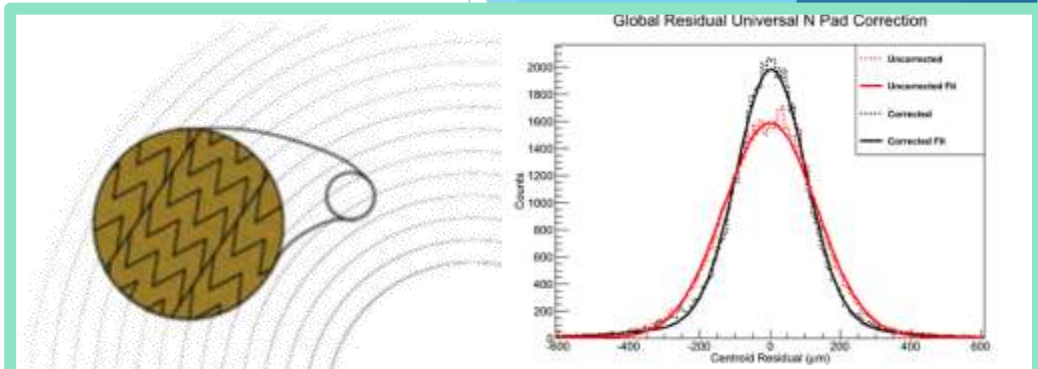

Better than 100 μm routine.

ALICE expected track deflection

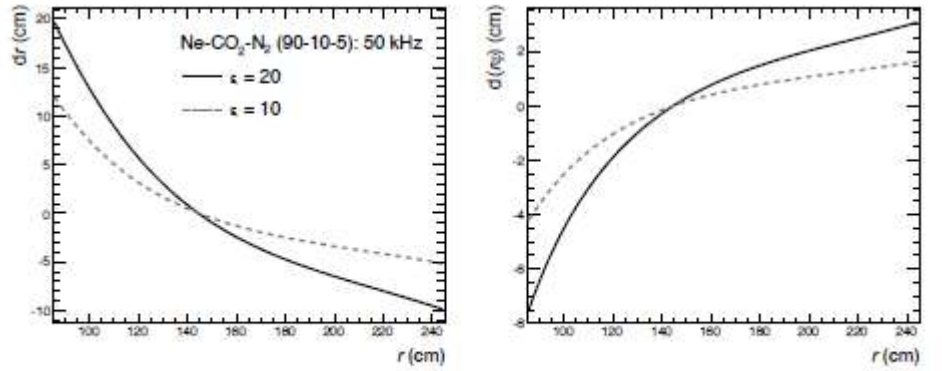

Figure 7.9: Space-point distortions in r (left panel) and $r\varphi$ (right panel) as a function of the radial position r close to the central electrode ($z \approx 0$ cm) for Ne-CO_2-N_2 (90-10-5), $R_{\mathrm{tot}} = 50$ kHz, $\varepsilon = 10$ and 20.

ALICE design goal: 200 μm from 4 mm pads.

Goal of the Study

- Make a (correct & precise) calculation of the mean deflections of ionization as they traverse the TPC.
- Apply all sources of fluctuations onto the full drift process.
  - Space charge, of course.
  - "Normal" fluctuations also!
- Add uncertainty in the full drift process to the uncertainty in the gain stage.
- Learn realistic resolution.

Mean Deflections of ionization due to space charge in ALICE @ 50 kHz

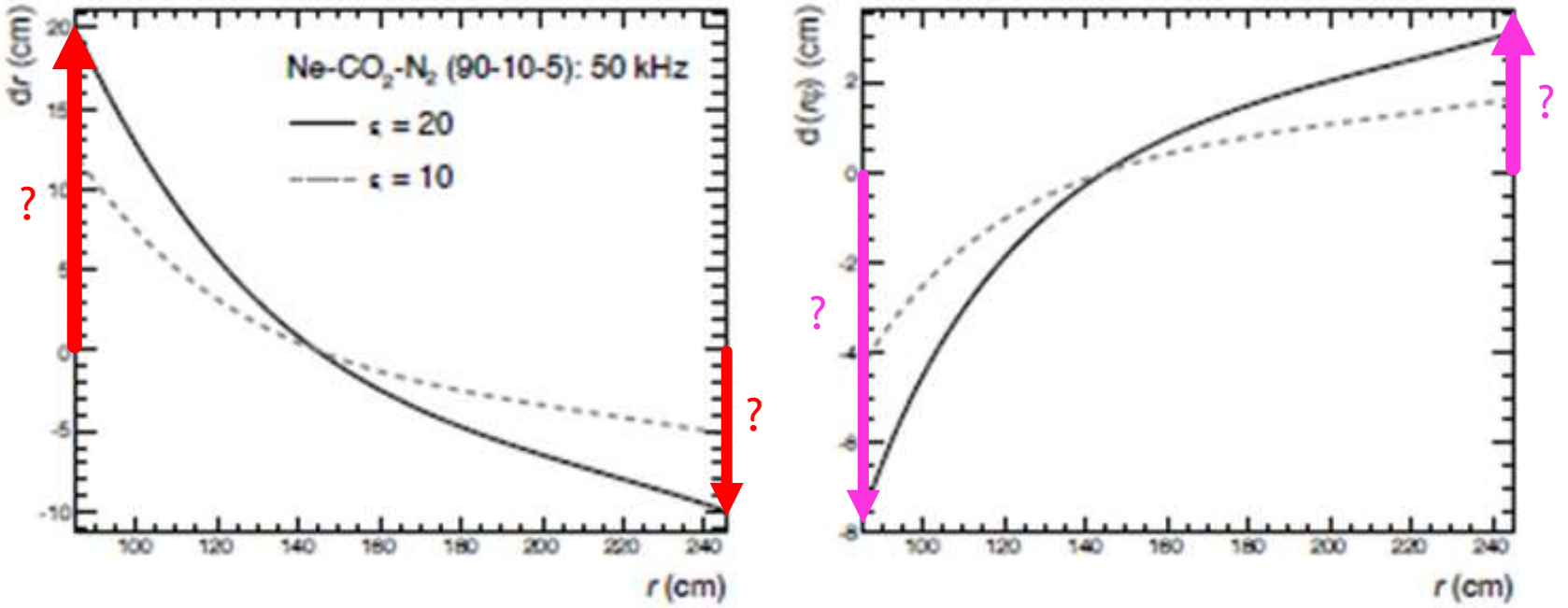

Figure 7.9: Space-point distortions in r (left panel) and $r\varphi$ (right panel) as a function of the radial position r close to the central electrode ($z \approx 0$ cm) for Ne-CO_2-N_2 (90-10-5), $R_{int} = 50$ kHz, $\varepsilon = 10$ and 20.

$$\Delta v_d = \left(\frac{\partial v_d}{\partial E}\Delta E + \frac{\partial v_d}{\partial T}\Delta T + \frac{\partial v_d}{\partial P}\Delta P + \frac{\partial v_d}{\partial C_{CO_2}}\Delta C_{CO_2} + \frac{\partial v_d}{\partial C_{N_2}}\Delta C_{N_2}\right).$$

ALICE

1^{st} order coefficients:		2^{nd} order coefficients:	
$\frac{\partial v_d}{\partial E}$	(0.24 ± 0.02) [% cm/V]	$\frac{\partial^2 v_d}{\partial E^2}$	-0.001 ± 0.009 [% cm/V]
$\frac{\partial v_d}{\partial T}$	(0.31 ± 0.02) [%/K]	$\frac{\partial^2 v_d}{\partial T^2}$	-0.001 ± 0.006 [%/K]
$\frac{\partial v_d}{\partial P}$	(-0.13 ± 0.01) [%/$Torr$]	$\frac{\partial^2 v_d}{\partial P^2}$	-0.001 ± 0.001 [%/$Torr$]
$\frac{\partial v_d}{\partial C_{CO_2}}$	(-6.60 ± 0.29) [%/%]	$\frac{\partial^2 v_d}{\partial C_{CO_2}^2}$	0.33 ± 0.95 [%/%]
$\frac{\partial v_d}{\partial C_{N_2}}$	(-1.73 ± 0.23) [%/%]	$\frac{\partial^2 v_d}{\partial C_{N_2}^2}$	0.15 ± 0.64 [%/%]

Implemented Code

Size as Constructor Argument

```
class Spacecharge
{
 public:
  Spacecharge(double a=30, double b=80, double L=80);
  virtual ~Spacecharge() {}

  void Verbosity(int v) {verbosity=v;}
  double Rmn (int m, int n, double r);  //Rmn function from Rossegger
  double Rmn1(int m, int n, double r);  //Rmn1 function from Rossegger
  double Rmn2(int m, int n, double r);  //Rmn2 function from Rossegger
  double RPrime(int m, int n, double a, double r);  // RPrime function from Rossegger

  double Rnk(int n, int k, double r);  //Rnk function from Rossegger

  double Ez   (double r, double phi, double z, double r1, double phi1, double z1);
  double Er   (double r, double phi, double z, double r1, double phi1, double z1);
  double Ephi(double r, double phi, double z, double r1, double phi1, double z1);

 protected:
```

Temporarily public (testing only)

Return Functions

- Ez and Er implementation are unchanged since last report.
- Help from Dave Morrison provides implementation necessary for Ephi.
  - Currently dummy since we'll start with phi-symmetric space charge.
- Returns are effectively Greene's Functions that provide a value of a field at (r,ϕ,z) in response to a point charge placed at (r_1,ϕ_1,z_1).
- To learn the total field, one must integrate the Greene's function over the charge:

$$\overrightarrow{E_r}(\vec{x}) = \int E_r\left(\vec{x},\overrightarrow{x'}\right)\rho\left(\overrightarrow{x'}\right)dV'$$

$$\overrightarrow{E_z}(\vec{x}) = \int E_z\left(\vec{x},\overrightarrow{x'}\right)\rho\left(\overrightarrow{x'}\right)dV' + 400\frac{V}{cm}$$

Requires Proof Matches ALICE!

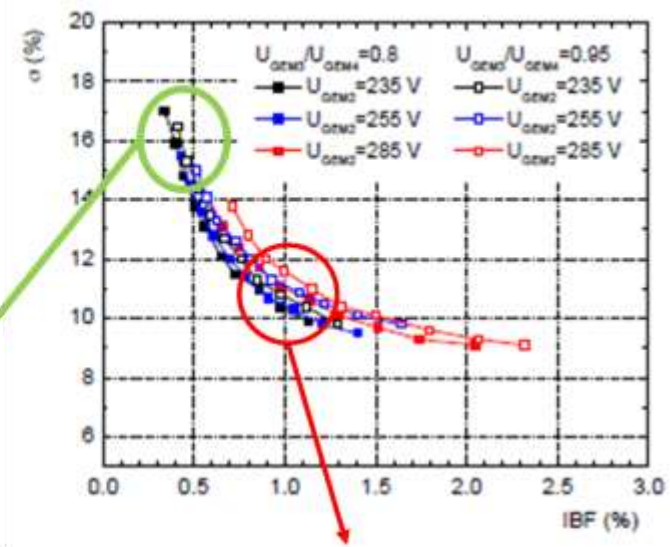

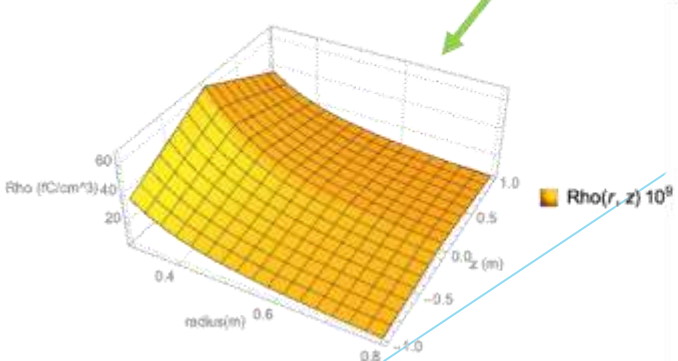

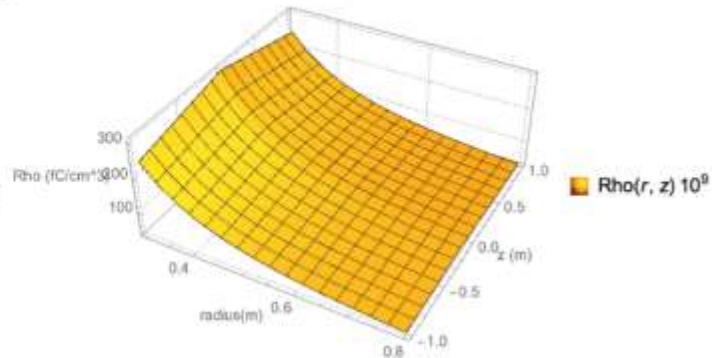

Factorization of the Space Charge Problem

Cylinder with graded potentials and space charge in the volume

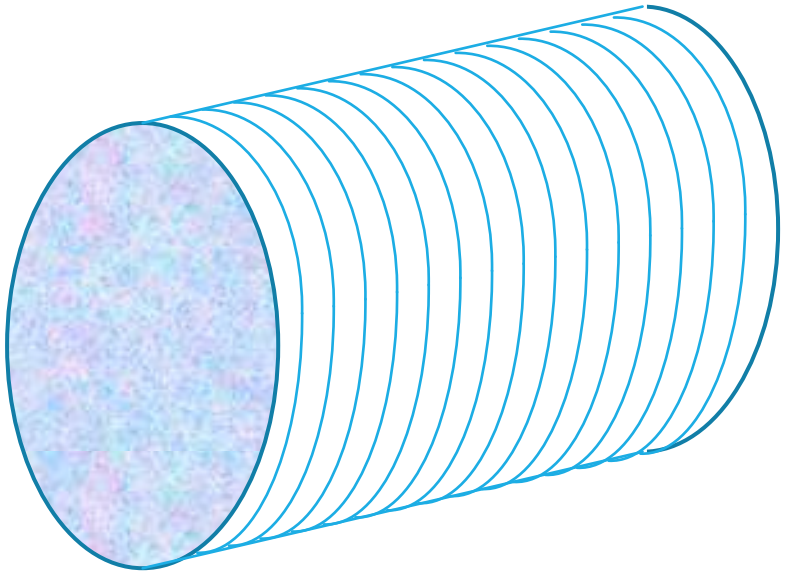

Grounded shell, + space charge

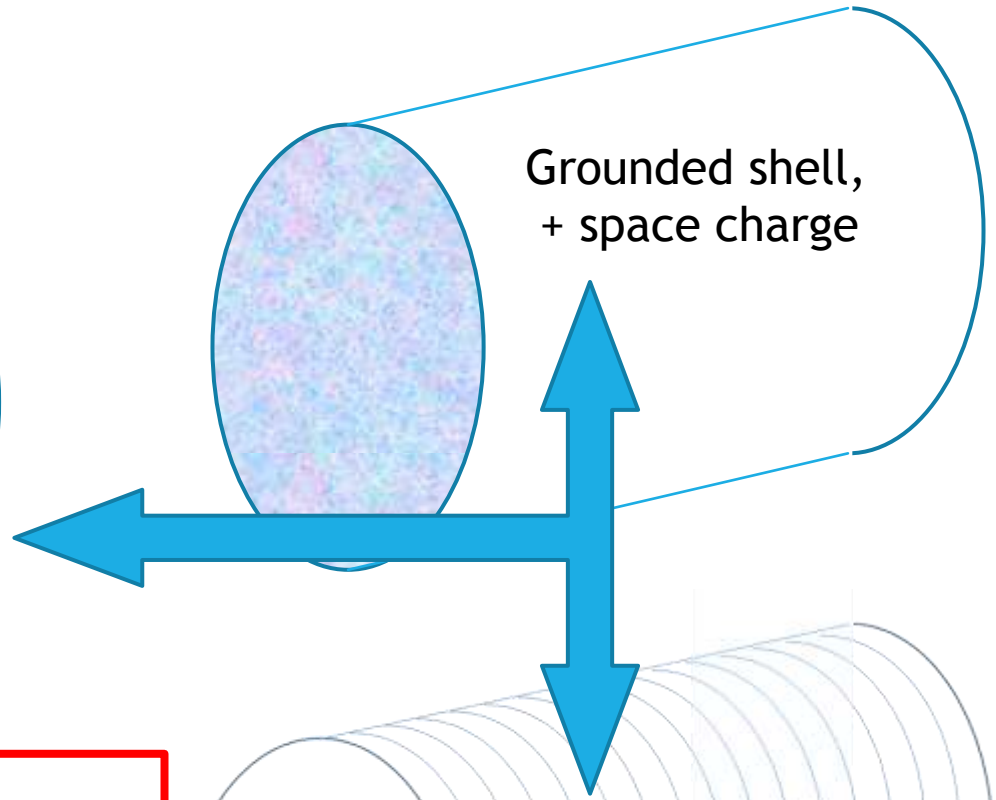

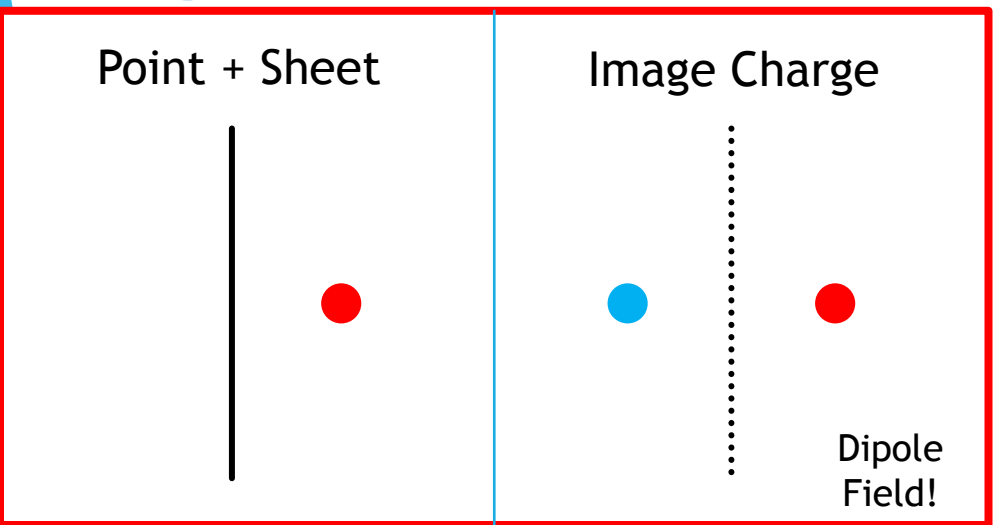

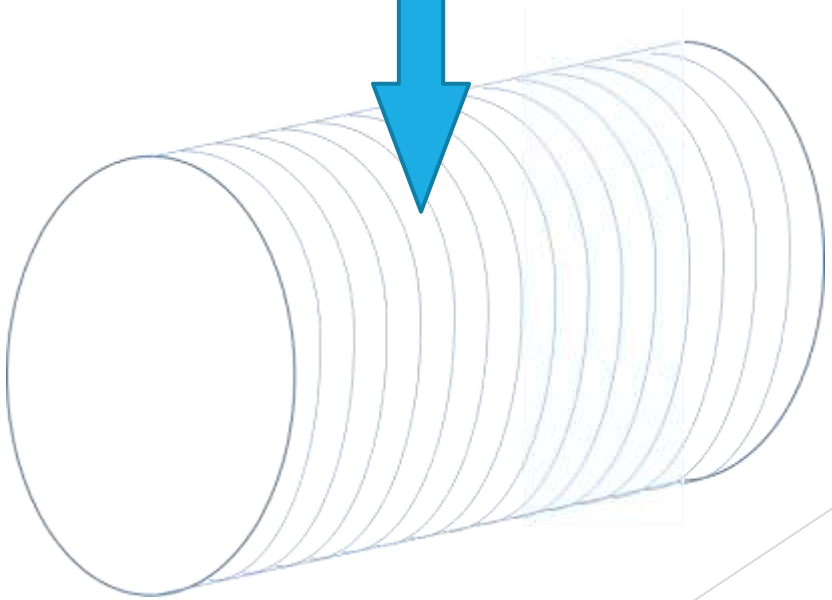

Graded potentials, no charge

- Graded field cage field determined by ANSYS or COLSOL finite element calculations.
- Grounded shell solved using Greene's theorem

$$\Delta G(\vec{r}, \overrightarrow{r_{ch}}) = \delta(\vec{r} - \overrightarrow{r_{ch}})$$

$$\overrightarrow{E_{ch}}(\vec{r}, \overrightarrow{r_{ch}}) = \vec{\nabla} G(\vec{r}, \overrightarrow{r_{ch}})$$

$$\vec{E} = \int \rho(\overrightarrow{r_{ch}}) \overrightarrow{E_{ch}}(\vec{r}, \overrightarrow{r_{ch}}) dV_{ch}$$

Carlos

Tom

Basic Approach to Solving the Cylinder

- The problem at hand is this:

$$\Delta G(\vec{x};\vec{x}') = -\delta(\vec{x}-\vec{x}'), \tag{5.13}$$

$$\left[\frac{\partial^2}{\partial r^2}+\frac{1}{r}\frac{\partial}{\partial r}+\frac{1}{r^2}\frac{\partial^2}{\partial \phi^2}+\frac{\partial^2}{\partial z^2}\right] G(r,\phi,z;r',\phi',z') = -\frac{\delta(r-r')}{r'}\,\delta(\phi-\phi')\,\delta(z-z'), \tag{5.14}$$

- Our solution begins with solving the homogeneous equation to provide a basis set of functions for the full solution:

$$\Delta\Phi = 0, \qquad \left(\frac{\partial^2}{\partial r^2}+\frac{1}{r}\frac{\partial}{\partial r}+\frac{1}{r^2}\frac{\partial^2}{\partial \phi^2}+\frac{\partial^2}{\partial z^2}\right)\Phi(r,\phi,z) = 0, \qquad \Phi(r,\phi,z) = R(r)\Phi(\phi)Z(z).$$

Periodicity set m=0,1,2,3,…

$$\Phi_m(\phi) = C_m\, e^{im\phi} = A_m\cos(m\phi) + B_m\sin(m\phi) \qquad \text{with } m \in \mathrm{Z}.$$

$$\frac{R_{rr}}{R}+\frac{1}{r}\frac{R_r}{R}-\frac{m^2}{r^2} = -\frac{Z_{zz}}{Z} = \begin{cases} -\beta^2, & \text{case I;} \\ \beta^2, & \text{case II}\,. \end{cases}$$

Solution without boundary conditions applied:

$$Z_m(z) = C_m\cosh(\beta z) + D_m\sinh(\beta z),$$
$$R_m(r) = E_m J_m(\beta r) + F_m Y_m(\beta r).$$

Constants formulated to explicitly vanish at r=a

$$R_{mn}(r) = Y_m(\beta_{mn}a)J_m(\beta_{mn}r) - J_m(\beta_{mn}a)Y_m(\beta_{mn}r).$$

Vanishing at r=b forces β to become discreet.

Finishing the solution

- Once the solutions to the homogeneous equation are known, we express the Dirac delta function in this basis:

$$\delta(\phi-\phi') = \frac{1}{2\pi}\sum_{m=-\infty}^{\infty} e^{im(\phi-\phi')} = \frac{1}{2\pi}\sum_{m=0}^{\infty}(2-\delta_{m0})\cos[m(\phi-\phi')],$$

$$\frac{\delta(r-r')}{r} = \sum_{n=1}^{\infty}\frac{R_{mn}(r)R_{mn}(r')}{\bar{N}_{mn}^2} \quad \text{with} \quad \bar{N}_{nm}^2 = \int_a^b R_{mn}^2(r)\, r dr,$$

$$m = 0, 1, 2, \ldots .$$

- After which the solution is readily obtained:

$$G(r,\phi,z;r',\phi',z') = \frac{1}{2\pi}\sum_{m=0}^{\infty}\sum_{n=1}^{\infty}(2-\delta_{m0})\cos[m(\phi-\phi')]\frac{R_{mn}(r)R_{mn}(r')}{\bar{N}_{mn}^2}\frac{\sinh(\beta_{mn}z_<)\sinh(\beta_{mn}(L-z_>))}{\beta_{mn}\sinh(\beta_{mn}L)}$$

- Although the solution is correct, it is not assured to be readily convergent.
- Rossegger used three independent basis sets to obtain stable, differentiable, convergent solutions for the r, ϕ, and z components of the field:

$$\frac{\partial}{\partial z}G(r,\phi,z,r',\phi',z') = \frac{1}{2\pi}\sum_{m=0}^{\infty}\sum_{n=1}^{\infty}(2-\delta_{m0})\cos[m(\phi-\phi')]\frac{R_{mn}(r)R_{mn}(r')}{N_{mn}^2}\frac{\partial}{\partial z}\left(\frac{\sinh(\beta_{mn}z_<)\sinh(\beta_{mn}(L-z_>))}{\beta_{mn}\sinh(\beta_{mn}L)}\right), \quad (5.64)$$

with $\frac{\partial}{\partial z}(\sinh(\beta_{mn}z_<)\sinh(\beta_{mn}(L-z_>))) =$

$$= \begin{cases} \beta_{mn}\cosh(\beta_{mn}z)\sinh(\beta_{mn}(L-z')), & \text{for } 0\le z<z'\le L, \\ -\beta_{mn}\cosh(\beta_{mn}(L-z))\sinh(\beta_{mn}z'), & \text{for } 0\le z'<z\le L. \end{cases}$$

$$\frac{\partial}{\partial r}G(r,\phi,z,r',\phi',z') = \frac{1}{\pi L}\sum_{m=0}^{\infty}\sum_{n=1}^{\infty}(2-\delta_{m0})\cos[m(\phi-\phi')]\sin(\beta_n z)\sin(\beta_n z')\frac{\partial}{\partial r}\left(\frac{R_{mn\,1}(r_<)R_{mn\,2}(r_>)}{I_m(\beta_n a)K_m(\beta_n b)-I_m(\beta_n b)K_m(\beta_n a)}\right), \quad (5.65)$$

with $\frac{\partial}{\partial r}(R_{mn\,1}(r_<)R_{mn\,2}(r_>)) = \begin{cases} R'_{mn}(a,r)R_{mn\,2}(r'), & \text{for } a\le r<r'\le b, \\ R_{mn\,1}(r')R'_{mn}(b,r), & \text{for } a\le r'<r\le b, \end{cases}$

wherein $R'_{mn}(s,t)$ is

$$R'_{mn}(s,t) = \frac{\beta_n}{2}\left(K_m(\beta_n s)(I_{m-1}(\beta_n t)+I_{m+1}(\beta_n t)) + I_m(\beta_n s)(K_{m-1}(\beta_n t)+K_{m+1}(\beta_n t))\right).$$

$$\frac{\partial}{\partial\phi}G(r,\phi,z,r',\phi',z') = \frac{1}{L}\sum_{k=1}^{\infty}\sum_{n=1}^{\infty}\sin(\beta_n z)\sin(\beta_n z')\frac{R_{nk}(r)R_{nk}(r')}{N_{nk}^2}\frac{\partial}{\partial\phi}\left(\frac{\cosh[\mu_{nk}(\pi-|\phi-\phi'|)]}{\mu_{nk}\sinh(\pi\mu_{nk})}\right) \quad (5.66)$$

with $\frac{\partial}{\partial\phi}(\cosh[\mu_{nk}(\pi-|\phi-\phi'|)]) =$

$$= \begin{cases} -\mu_{nk}\sinh[\mu_{nk}(\pi-(\phi-\phi'))], & \text{for } 0\le\phi'<\phi\le 2\pi \\ \mu_{nk}\sinh[\mu_{nk}(\pi-(\phi'-\phi))], & \text{for } 0\le\phi<\phi'\le 2\pi \end{cases}$$

Gauss' Law Test

$$\oint \vec{E} \cdot \overrightarrow{dA} = \frac{Q_{in}}{\epsilon_0}$$

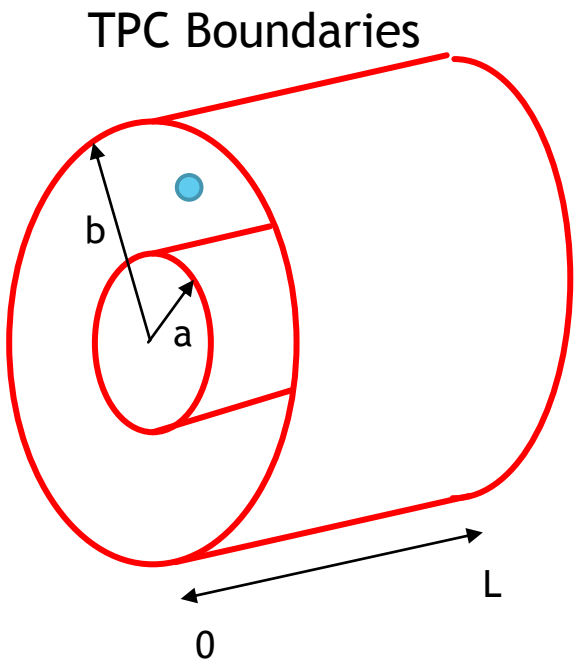

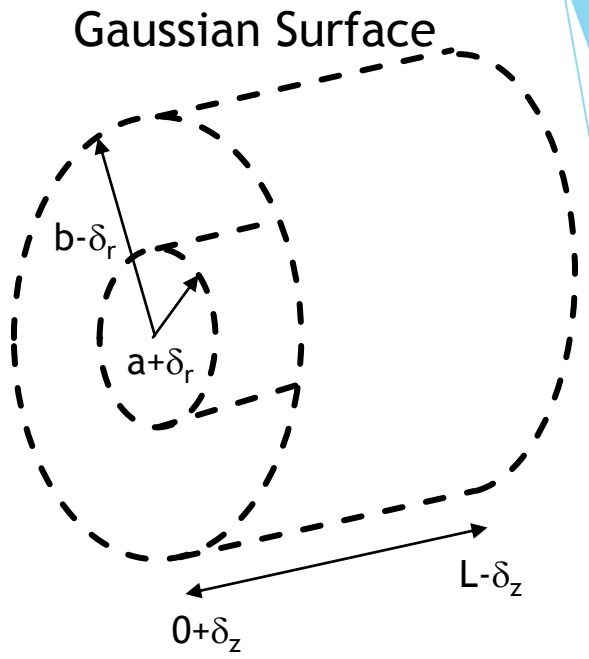

- Place single point charge.
- Gaussian surface "interior" by δ_r and by δ_z.
- Integrate Gauss' Law vs δ_r and by δ_z.
- Expectation:
  - Constant while charge enclosed.
  - Zero when charge excluded.
- Integral negative due to dropping minus:

$$\vec{E} = -\vec{\nabla} V$$

Test of E_r

$\oint \vec{E} \cdot \overrightarrow{dA}$

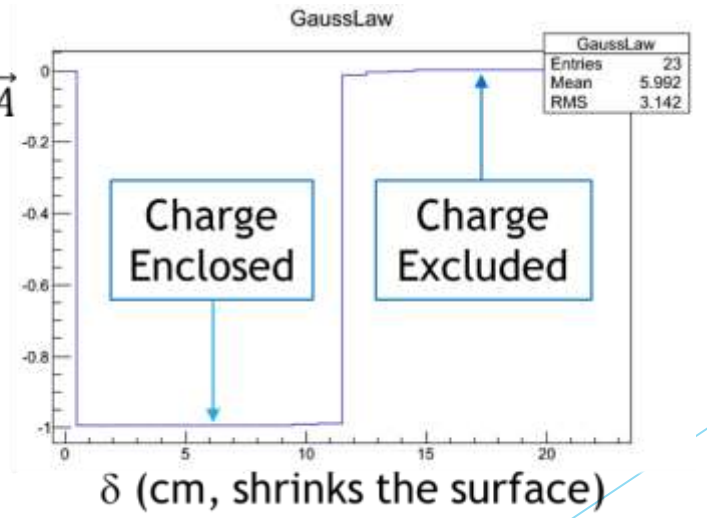

Test of E_z

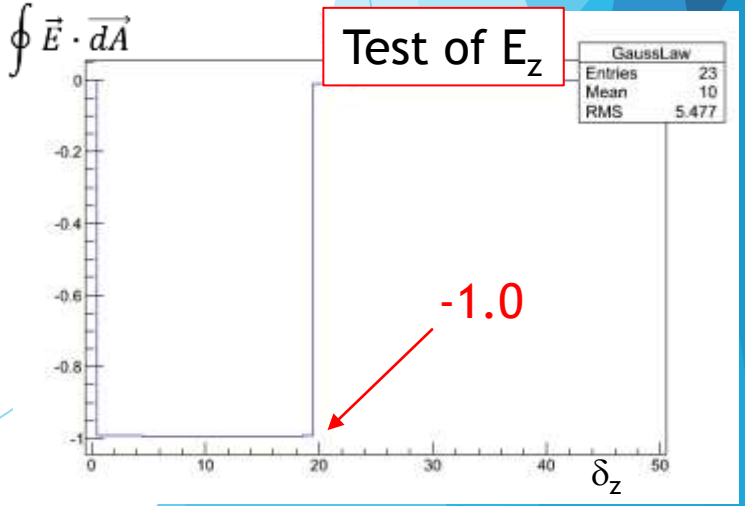

“Sanity Check”

- Basic shape of the field components looks very similar to ALICE and matches physical intuition.
- This is not yet proof that the implementation of the functions is:
  - Robustly correct.
  - Produces an answer on a known scale (V/cm is neither mks nor cgs).
- Test the implementation by confirming that the result obeys Gauss’ Law!

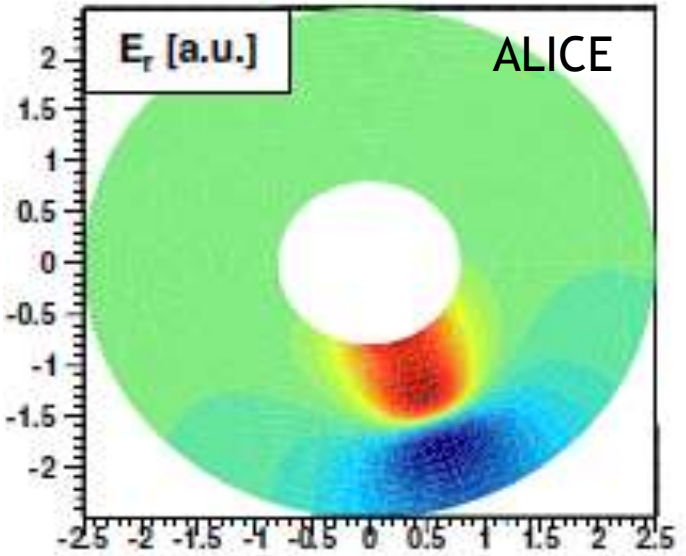

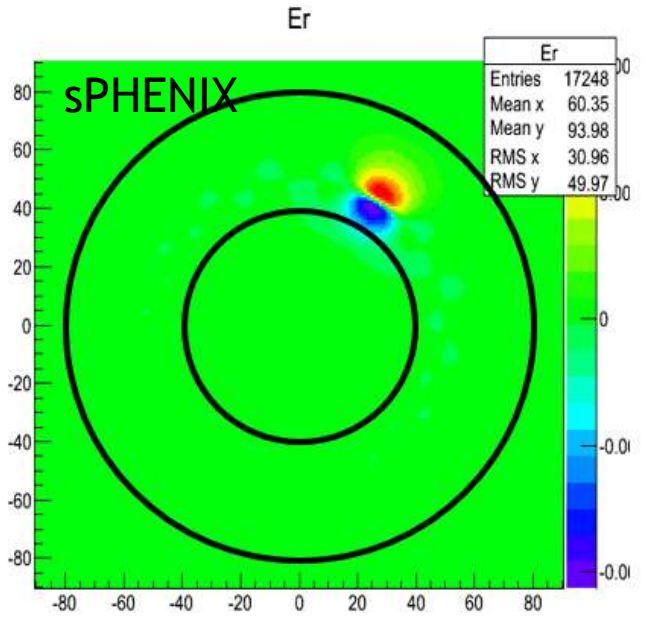

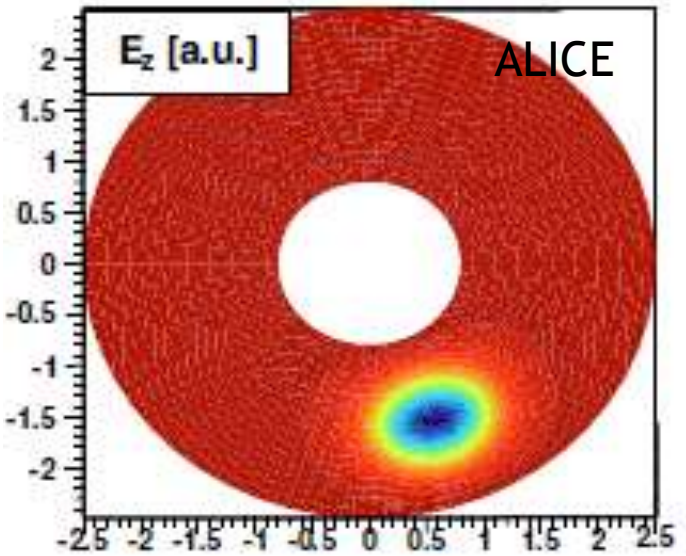

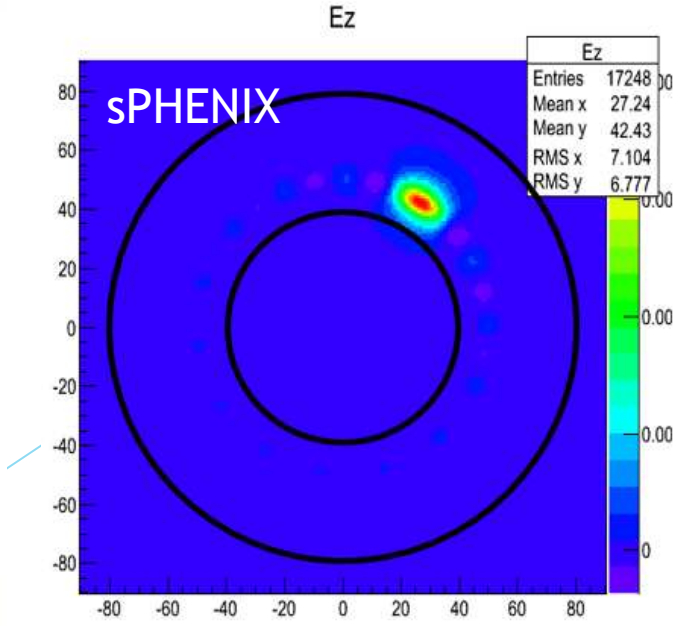

How to Make This Plot:

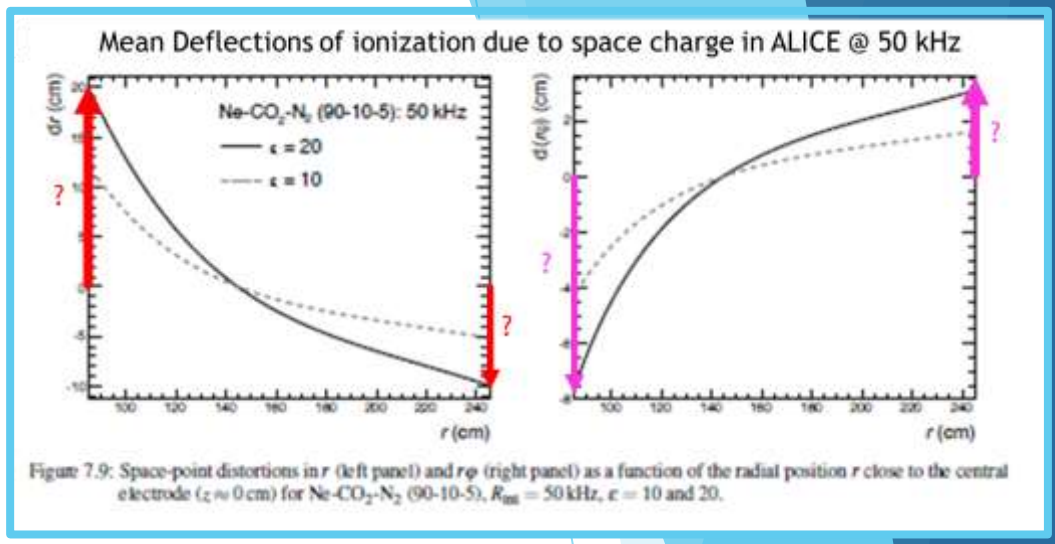

Figure 7.9: Space-point distortions in r (left panel) and $r\varphi$ (right panel) as a function of the radial position r close to the central electrode ($z \approx 0$ cm) for Ne-CO_2-N_2 (90-10-5), R_{ion} = 50 kHz, ε = 10 and 20.

- Choose an IBF operating point and collision rate (raw not triggered)
- Use standard form for the space charge density under these conditions.
- Select r=a.
- Integrate:

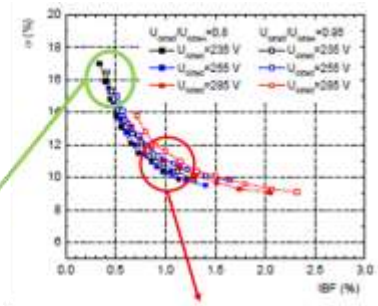

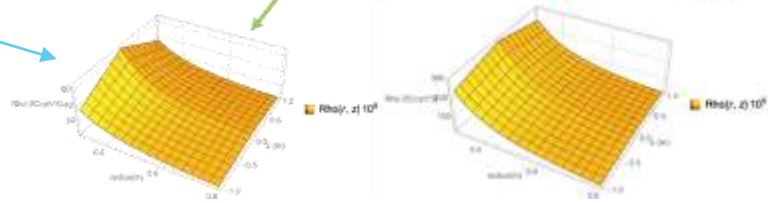

$$dr = \int \frac{E_r}{E_z} dz = \int \frac{\int E_r\left(\vec{x}, \overrightarrow{x'}\right) \rho\left(\overrightarrow{x'}\right) dV'}{400 \frac{V}{cm} + \int E_z\left(\vec{x}, \overrightarrow{x'}\right) \rho\left(\overrightarrow{x'}\right) dV'} dz$$

- DAMNED SLOW CALCULATION…
- We will leave Carlos' job running (single CPU) and launch a parallel effort to develop a fast calculation:
  - Use pre-tabulated results and interpolation in place of Bessel function calls.
  - Split the job so that it runs on many CPUs.

Current Result: Max Deflection = 3 cm
Requires further vetting to prove that it is robust…

Aces in the Hole

- The Baseline sPHENIX program does NOT require dE/dx from the tracker.
- We can select an operating point that favors low IBF for heavy ion collisions and then regain dE/dx for EIC simply by changing the voltages.
- We can choose a lower initial ionization gas (already must go to Ne…He is also possible).
- We can operate using gasses that are more forgiving (Ne CO_2 is NOT on the velocity plateau) of imperfections in temperature/field.
- We can “hedge” the IBF issue by moving the internal window inward (remember, deflection due to relative space charge).

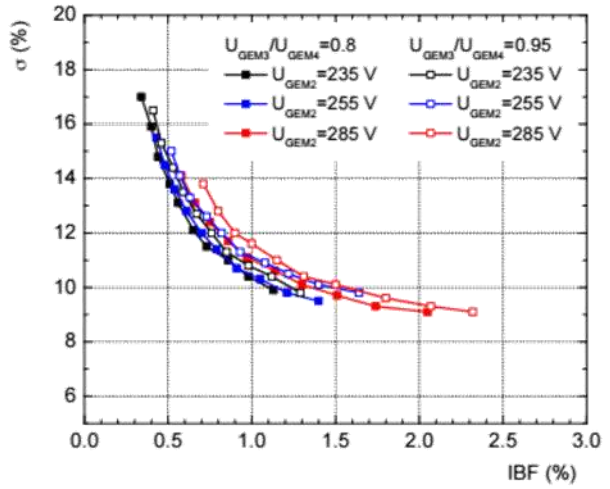

Figure 5.4: Correlation between ion backflow and energy resolution at 5.9 keV in a quadruple S-LP-LP-S GEM in Ne-CO_2-N_2 (90-10-5) for various settings of ΔU_{GEM2}. The voltage on GEM 1 increases for a given setting between 225 and 315 V from left to right. The voltages on GEM 3 and GEM 4 are adjusted to achieve a total effective gain of 2000, while keeping their ratio fixed. The transfer and induction fields are 4, 2, 0.1 and 4 kV/cm, respectively.

TPC R&D

TK Hemmick

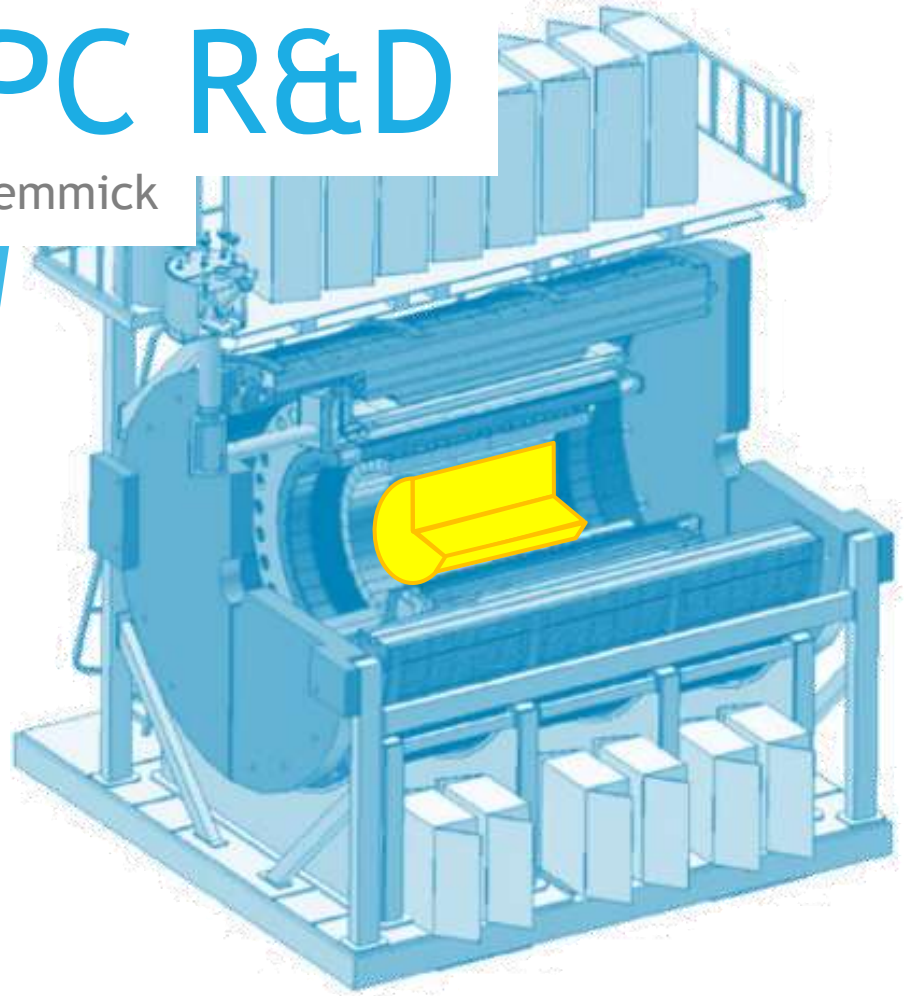

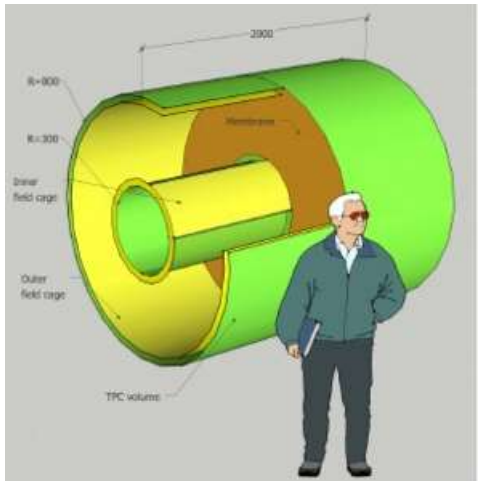

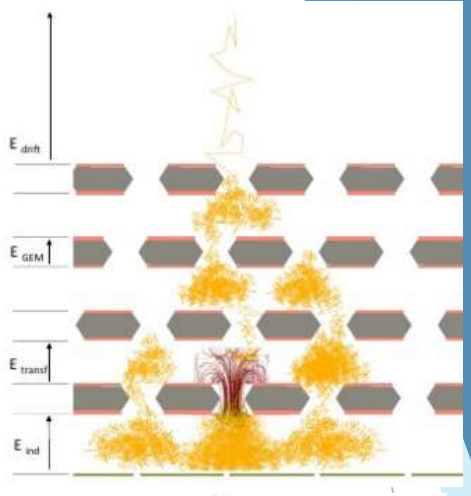

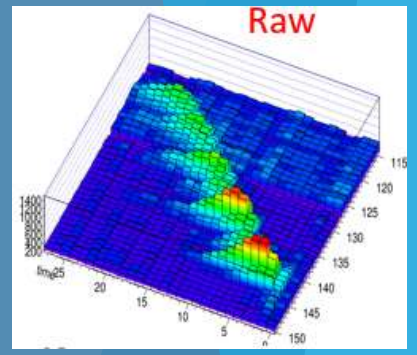

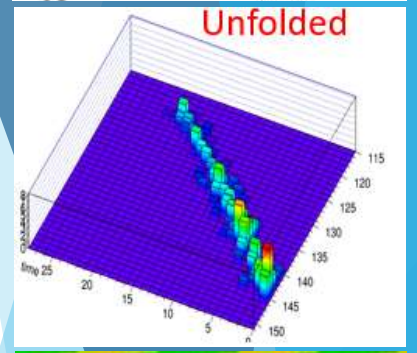

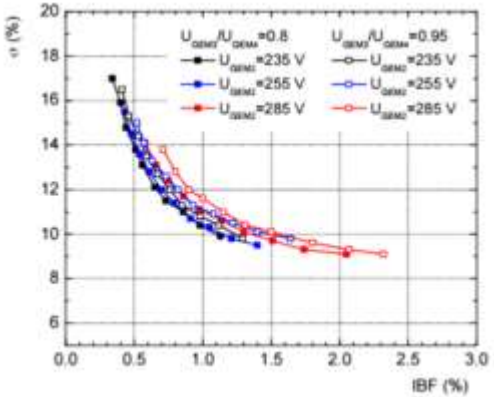

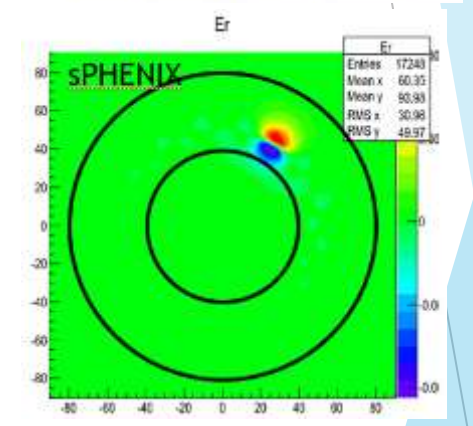

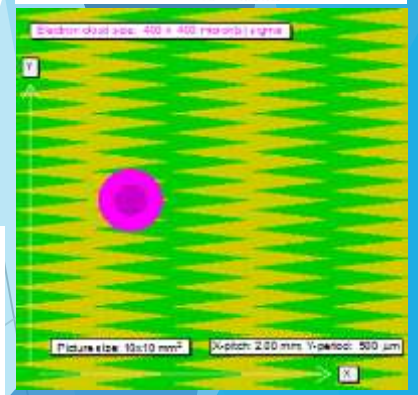

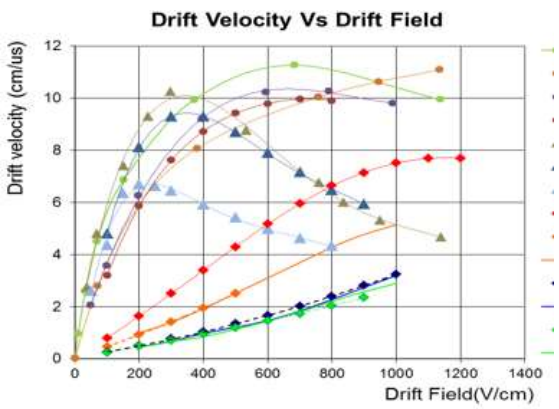

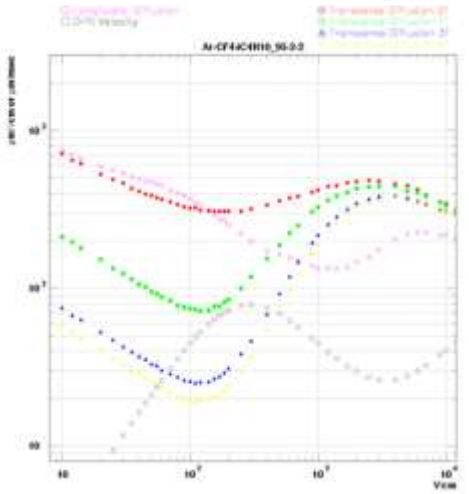

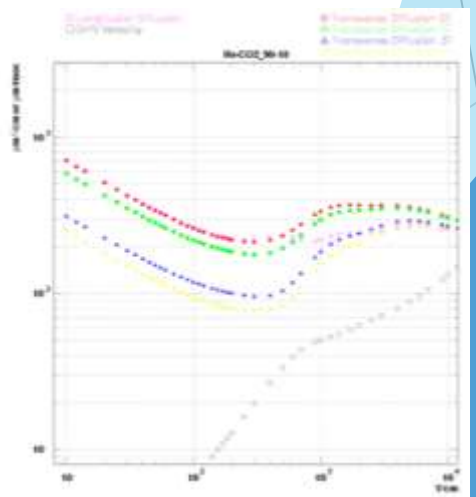

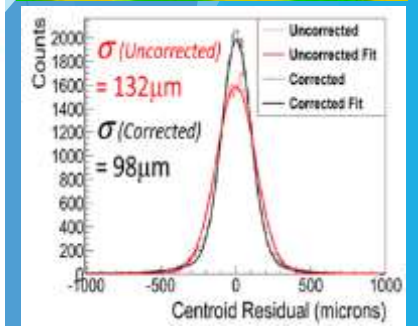

eRD6 – EIC R&D

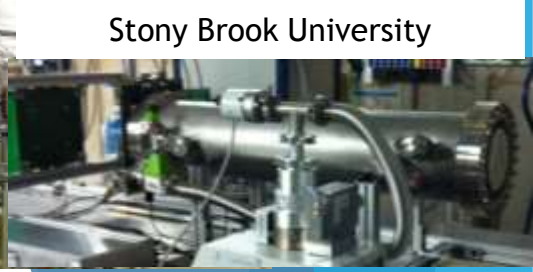

- "Tracking/PID Consortium"
  - BNL, FIT, UVa, SBU, Yale (LLNL, TU, WIS)
  - Varied R&D topics w/ MPGD devices:
    - Mini-drift pad chambers.
    - Chevron readout
    - TPC/HBD prototype
    - Large-scale/Low mass GEM trackers
    - CsI RICH for High-momentum PID
    - 3-coordinate pad readout
    - Hybrid gain stage for low IBF TPC devices
- Staged large test beam expt @ FTBF

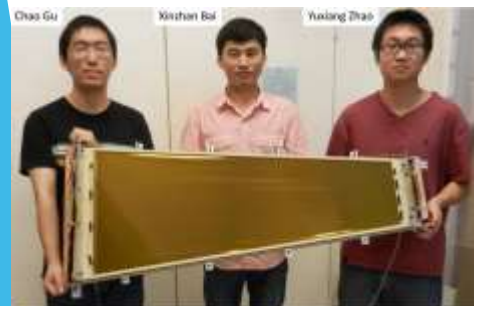

Largest Compass-style Chamber

3-coords from single foil

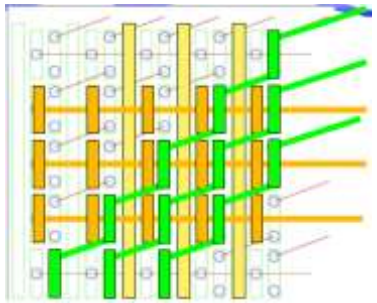

Assorted eRD6 Results (most published)

RICH-based PID

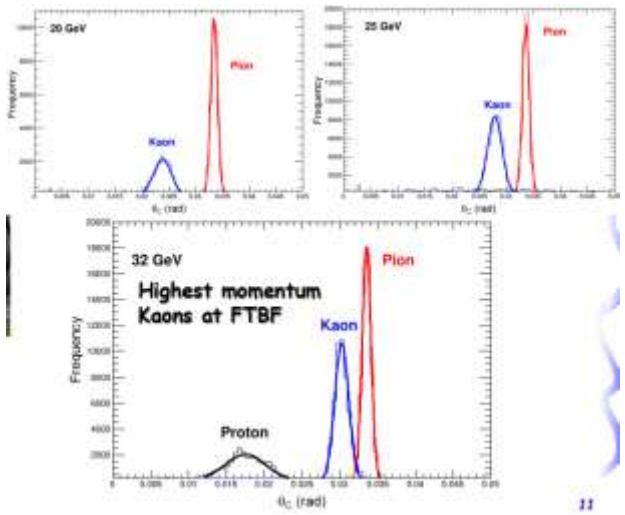

Large Chamber w/ small angle stereo

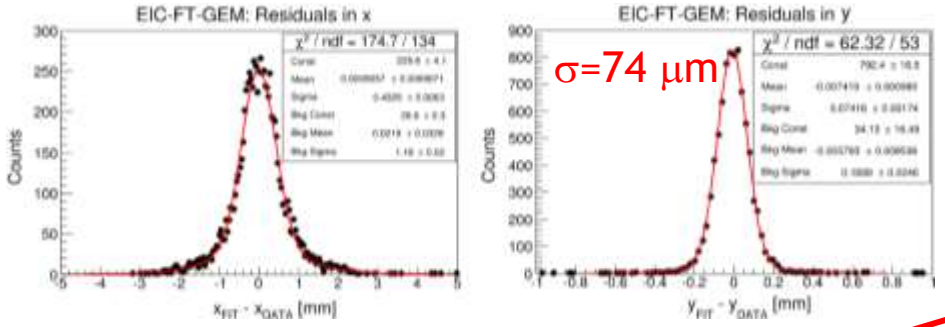

Small TPC w/ Chevrons

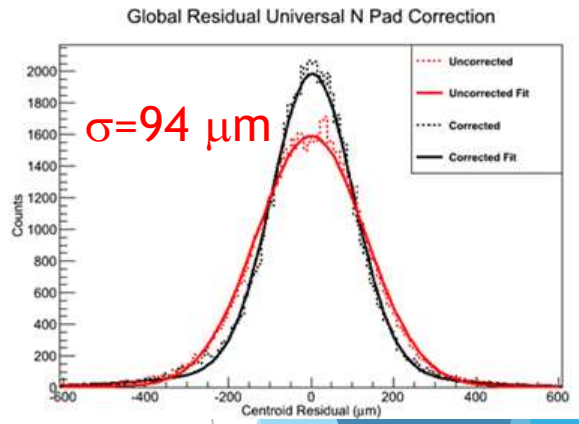

Most relevant to us?

3-coordinate

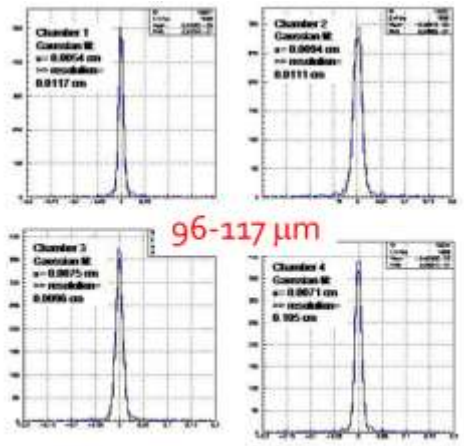

IBF with Hybrid Gain Stage

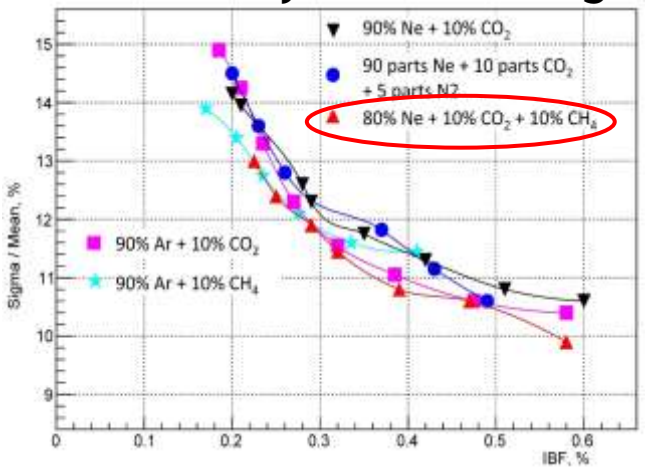

H. Wieman Grid simulation

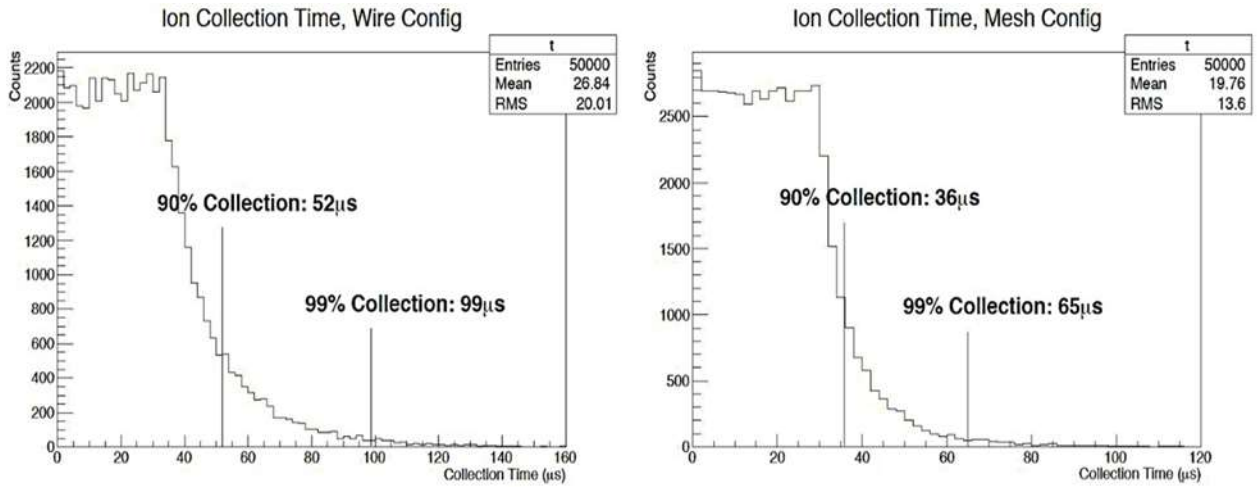

Facilities at BNL (co-occupied by Yale)

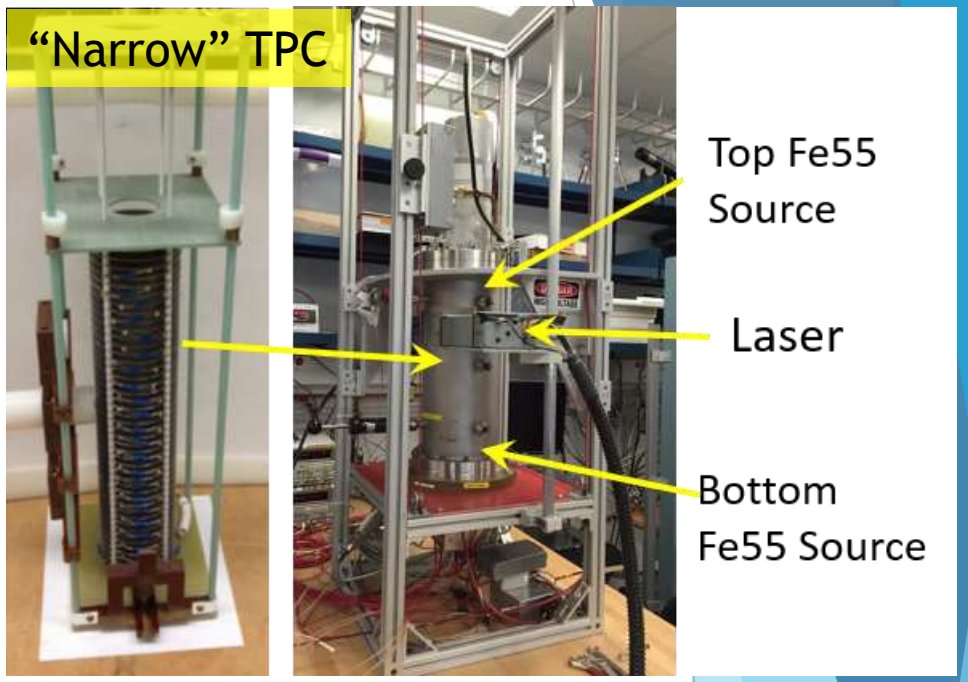

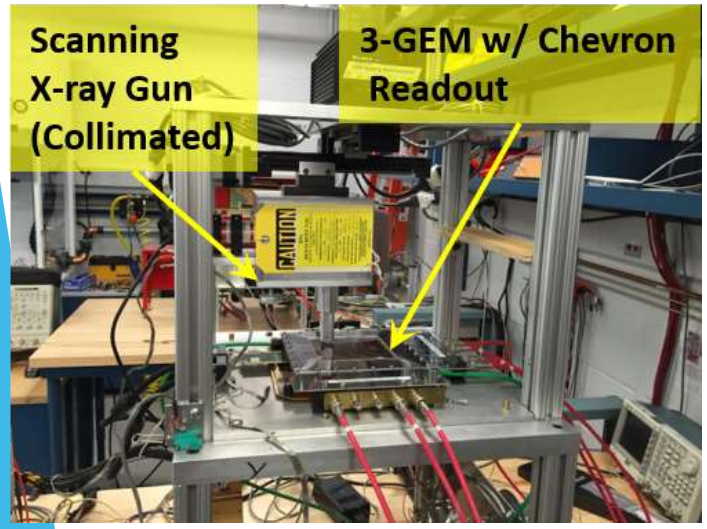

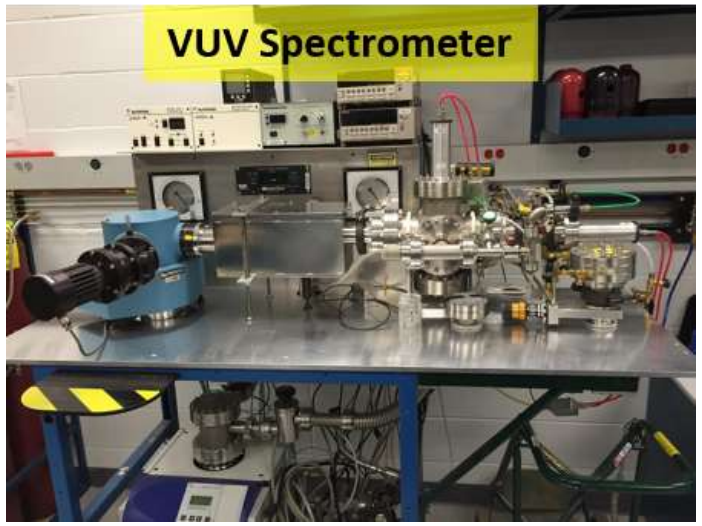

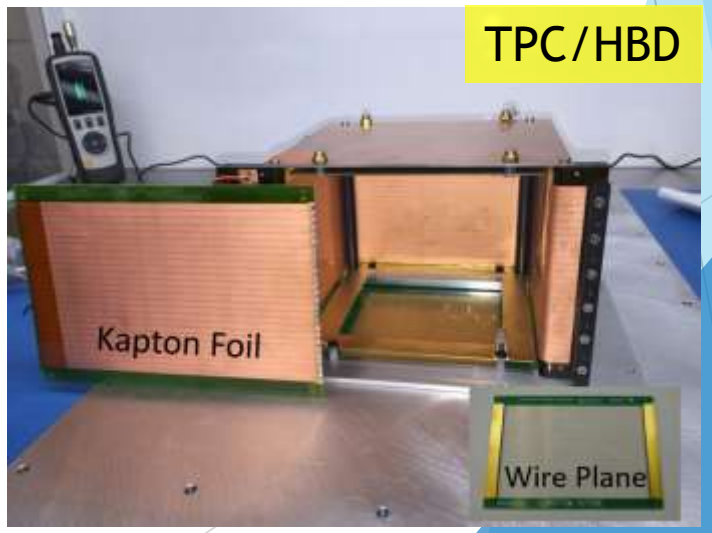

Facilities at WIS

IBF test box

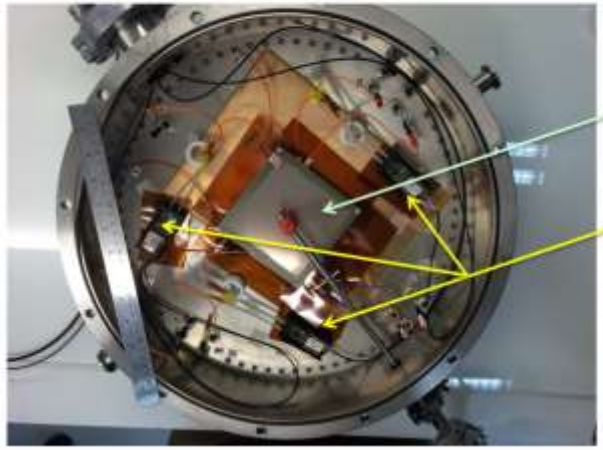

It has new inhabitants:

Standard 3(expandable) framed CERN GEMs

Zagreb-made floating picoampermeters.

They are sensitive to measure current from a 5kHz iron source. (Signals are weak).

Zagreb pA's

www.picologic.hu

Battery powered or DC powered.

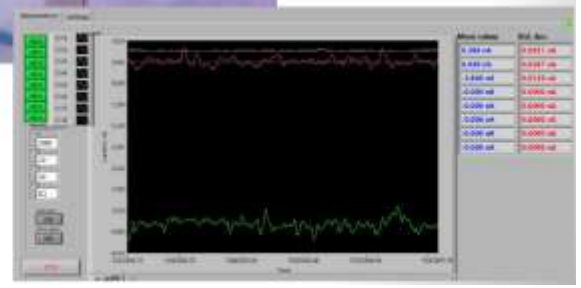

Gas system

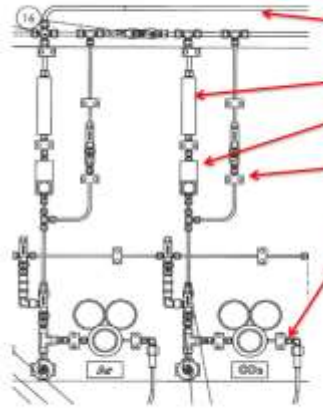

3 output lines (2 shown)
Configurable
Visual control
Fully computer controlled
2% accuracy
Fast fill up
4 input lines
(two shown)

The clean room.

New test cell

Assembly of 10x10cm CERN GEMs
View ports, laser injection window
Field cage
Lens and mirrors for 266nm
Radioactive source
Vacuum ports
HV feed through
Linear transformer

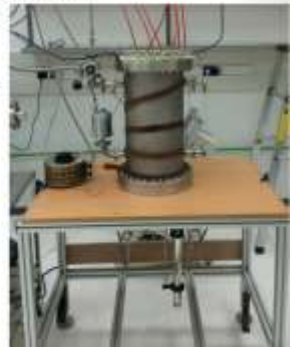

- Complete capabilities for gas characterization & IBF.
- BTW—Yale and SBU are not exactly devoid of relevant equipment

Basic Concept

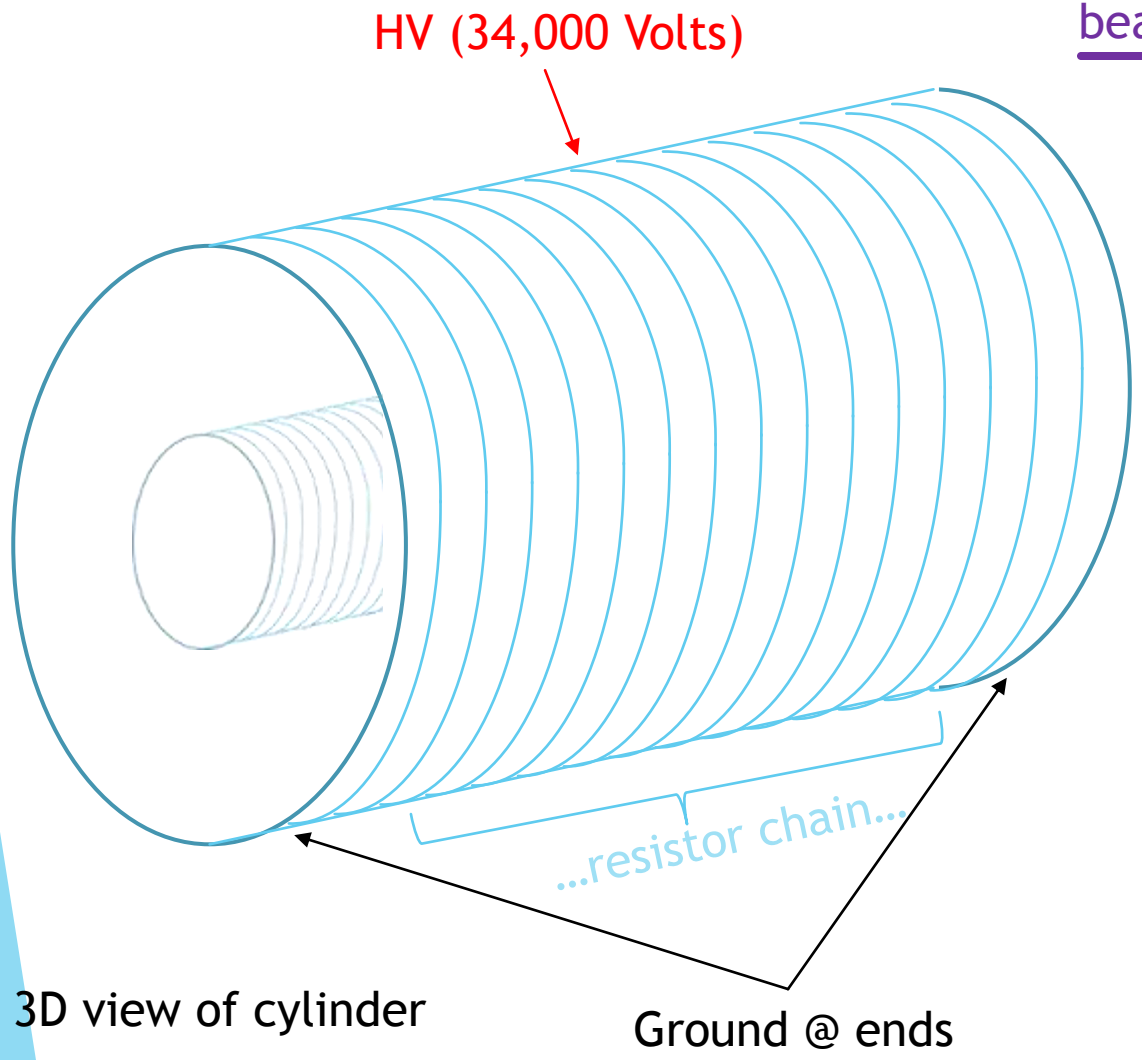

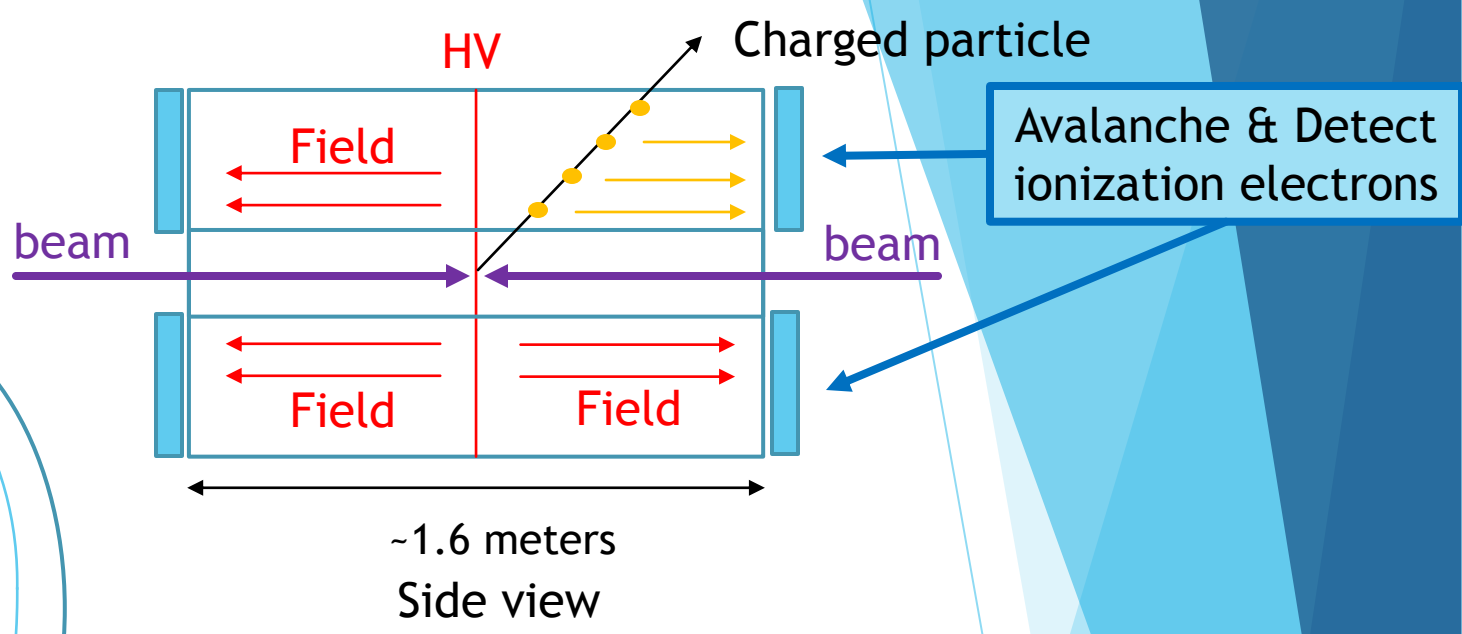

- Field Cage role in the overall process:
  - Provide the UNIFORM electric field.
  - Support the avalanche detectors
  - Services:
    - Gas in/out; HV in; Electronics support; Laser
- Strategy for sPHENIX:
  - Design/build FINAL field cage during prototyping.
    - Groundbreaking tech is mostly in the avalanche stage.
    - MPGD devices challenging to work at full size.
  - Move some cost & risk off-project.

Cartoons for terminology

STAR Terminology:

End View:

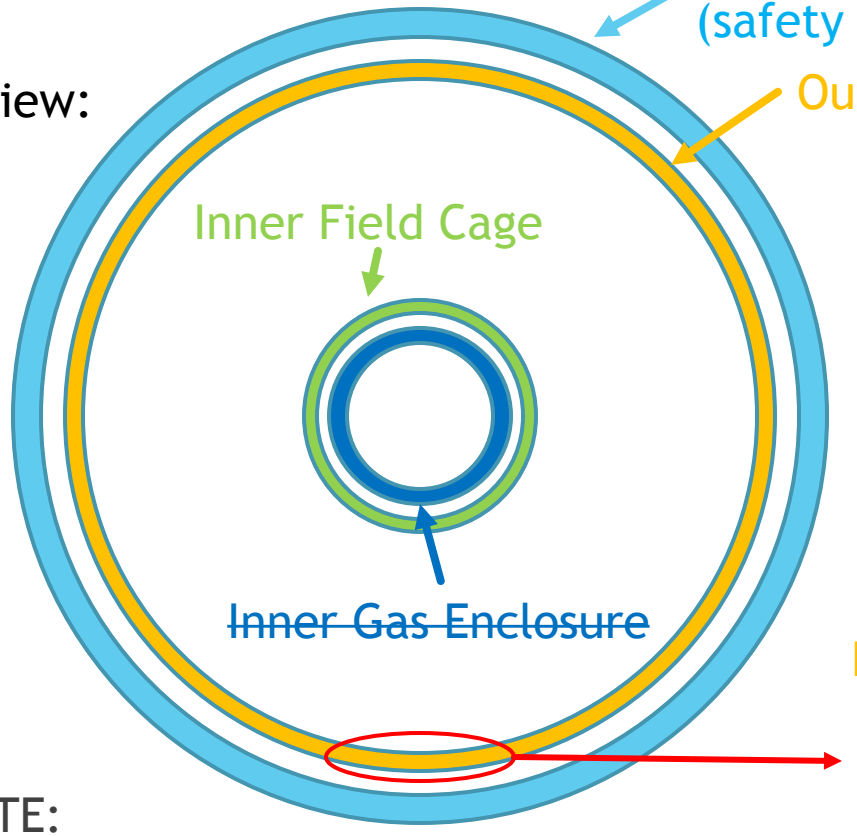

Kapton or FR4
Hexcell Honeycomb (1cm - 1/2”)
Kapton or FR4

Side View:

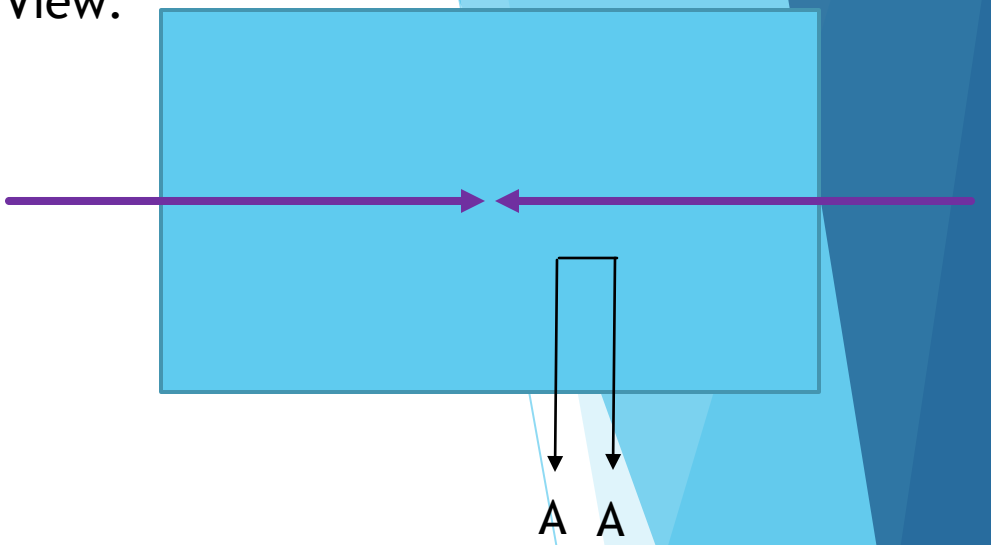

A:A

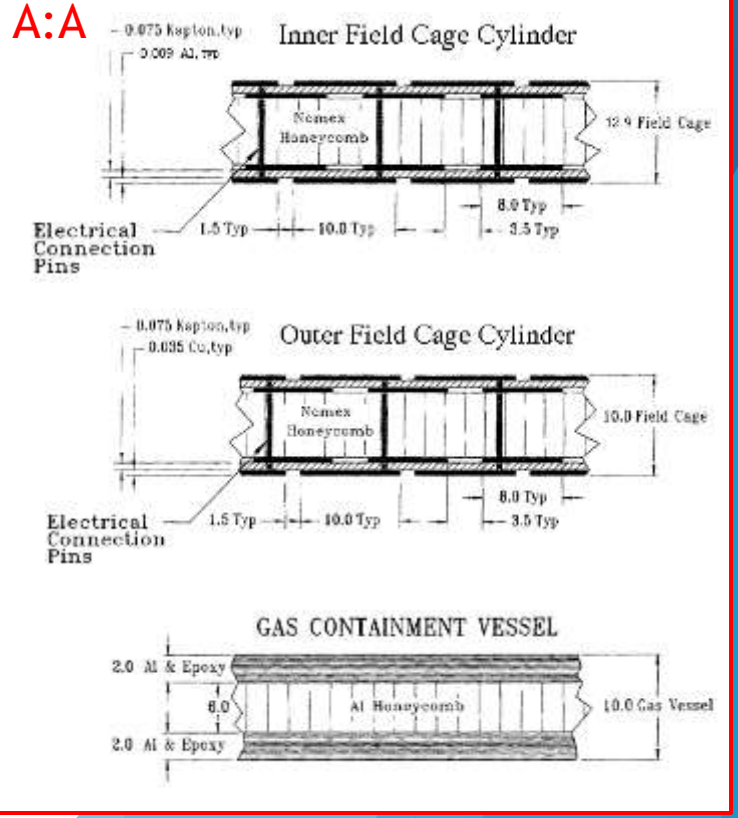

NOTE:

- STAR skipper the inner gas enclosure.
- Advice: Don’t copy that mistake.

More Cartoons for terminology

ALICE Terminology:

End View:

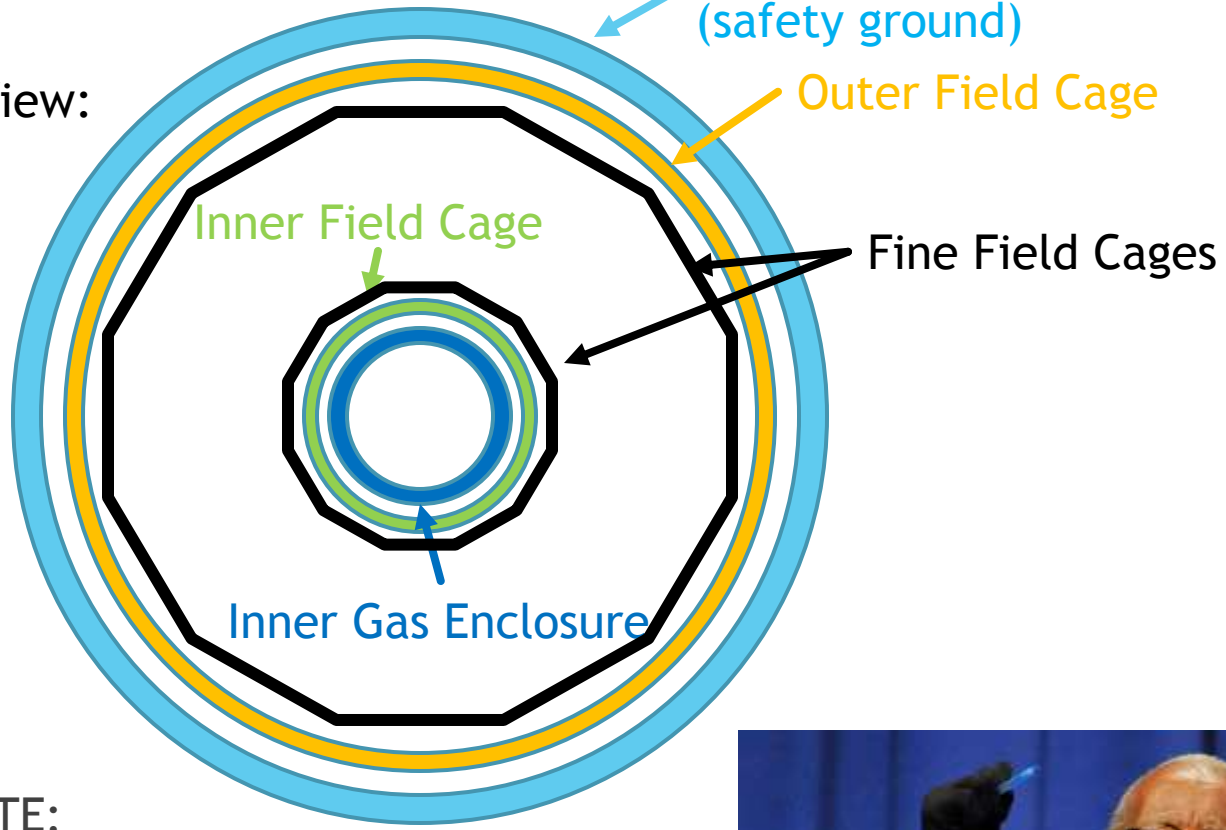

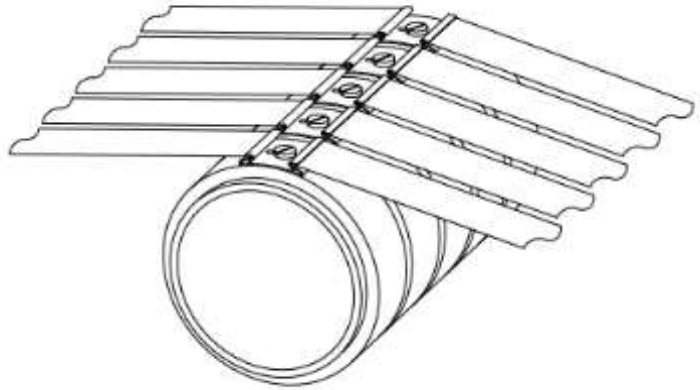

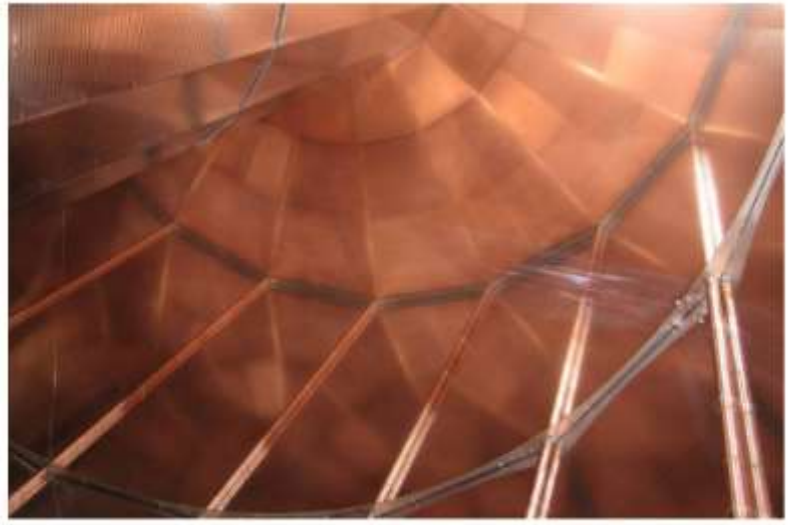

NOTE:

- ALICE adds fine field cage.
- We don't have room!

Fine Field Cages use too much damn room

STAR uses an air gap:

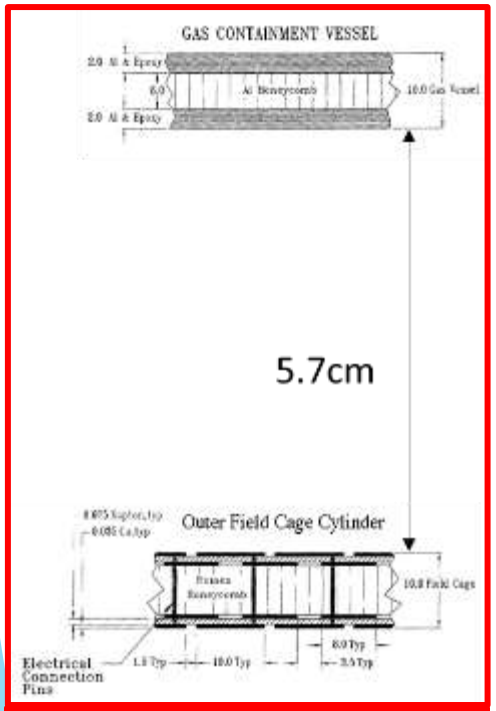

Drawing **IS** to scale.

- STAR used a 5.7 cm gap holding a maximum voltage of 27 kV.
- They flowed nitrogen through the gap.
- Overall thickness is 7.7cm.
- Using the same considerations, we would design:
  - $Gap = 5.7cm \frac{34000\ Volt}{27000\ Volt} = 7.2\ cm$
  - With 1cm for each honeycomb = 9.2 cm.
  - This is 3.6 inches (4X too large).

Losing 7-9 cm in a device this big is OK for STAR…but not for us!

Design concept for full field cage.

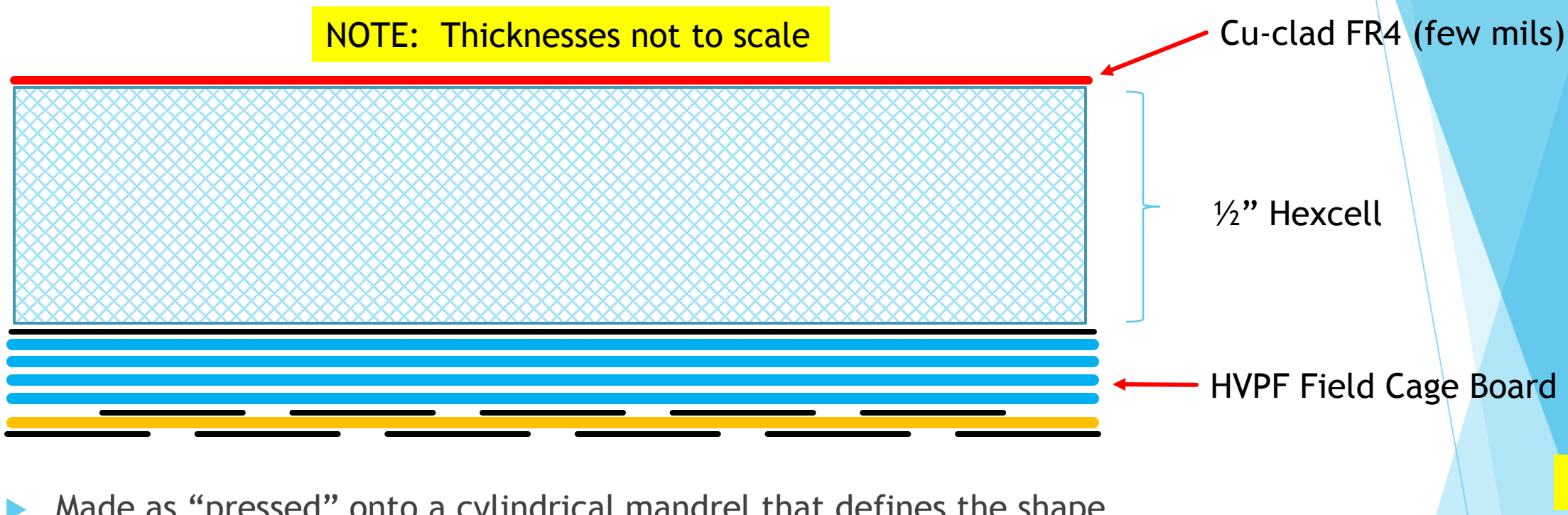

- Made as "pressed" onto a cylindrical mandrel that defines the shape.
- 1mm of kapton is ~0.3% of a radiation length.
- Shielded HV cable that holds 100 kV is 0.4" diameter (fits inside hexcell).
- Resistor chain inside the gas (like STAR & ILC).
- Test a flat prototype in the tandem injector cage.

Figure 11: Materials Supported in Multilayer High Voltage

Material Type	Max. Operating Temperature (°C)	T/G °C	Voltage (V/mil) Note 1	Aged rating (V/mil)	W°C/m
FR4	105-130	160	800	300/150	0.21
FR4 Hi-Temp.	130-150	170	800	300/150	0.22
BT Epoxy	140-160	180	1300	600/400	0.40
Polyimide	150-190	200	900	700/500	0.25
HVPF*	180-200	210	3000 to 7000	3000/2000	0.28

*HVPF is a trademark of Sierra proto express.

VERY similar to ILC:

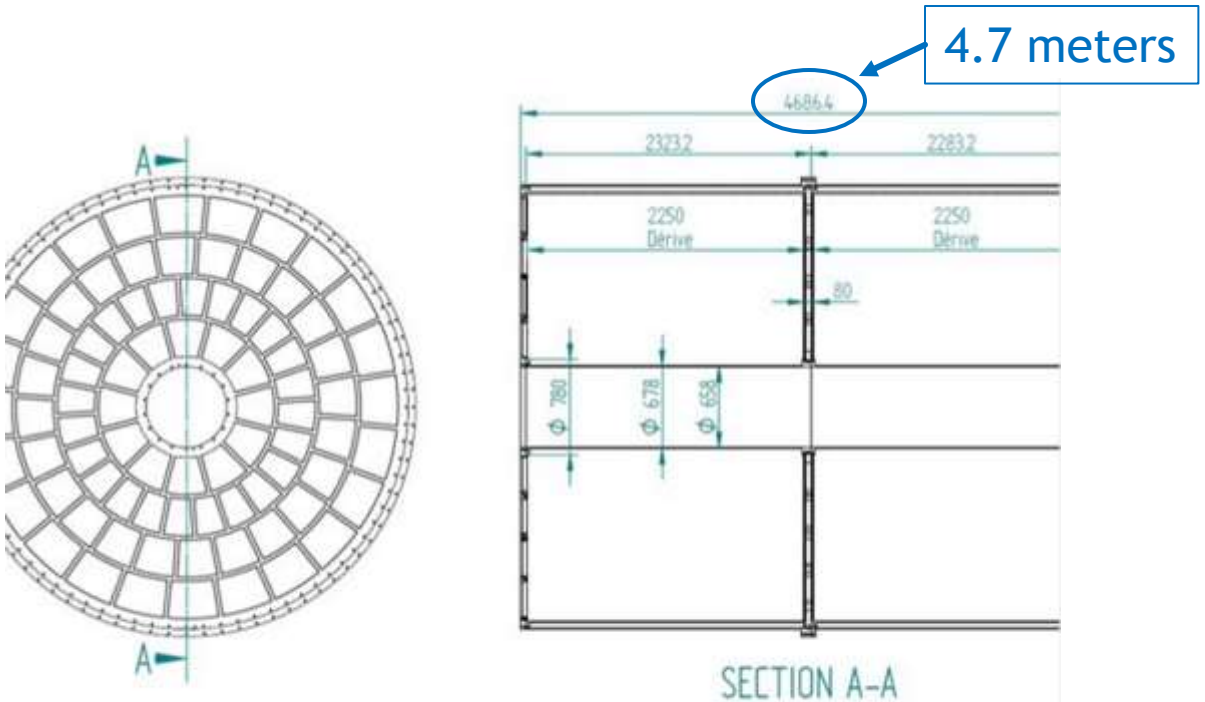

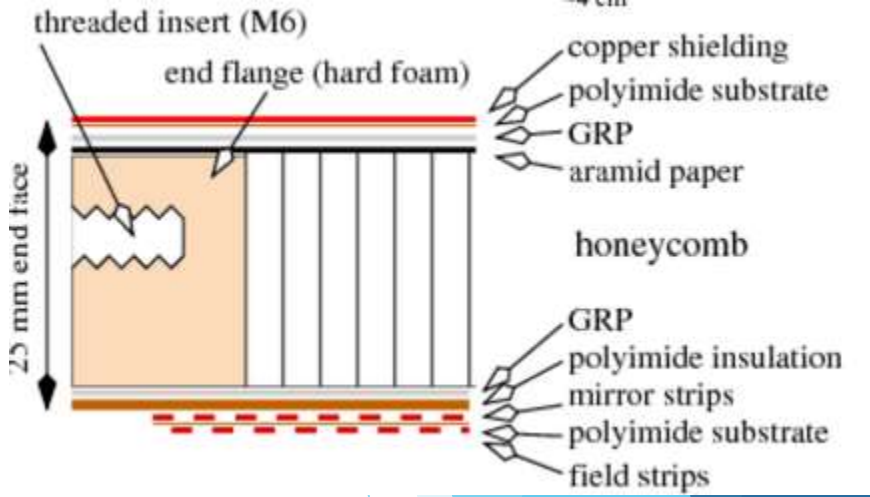

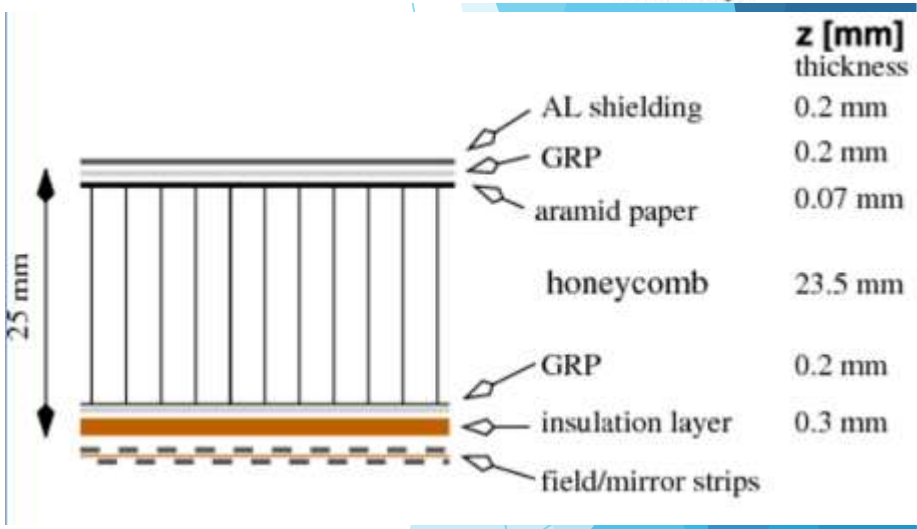

- Sized between STAR & ALICE.
- Does not use the “fine field cage”.
- Combines the field cage & gas enclosure into a single layer.

CONCLUSION:
- Our design will be a field cage and ground layer as a single unit.
- Need R&D for the specifics of the design…

HV test card design

Board shall be named “TPC HV TB–Rev 0”

Flexible

1. Test to destruction.
2. Irradiate…test again.

Multiple layers
3-4 mils per layer
Kapton adhesive/kapton layers
Laminated to final thickness.
Etch out the copper
Followed by ENIG

Gerber files…

30 pieces
50 pieces.
Turn time 10 days
8” by 8”
No vias

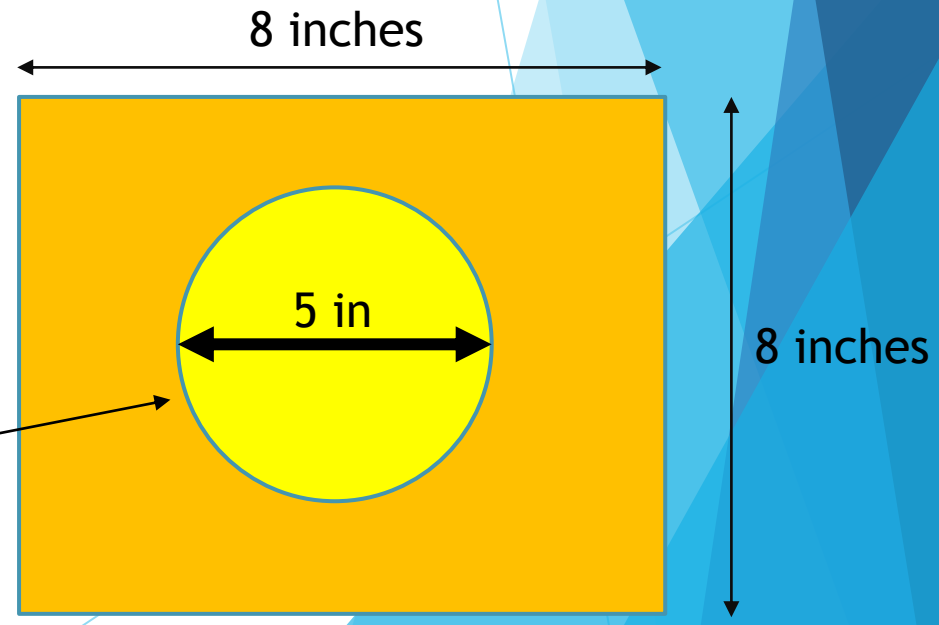

Minimum bend radius should be 20 cm

1mm thick material is required to withstand 40 kV

Under Voltage

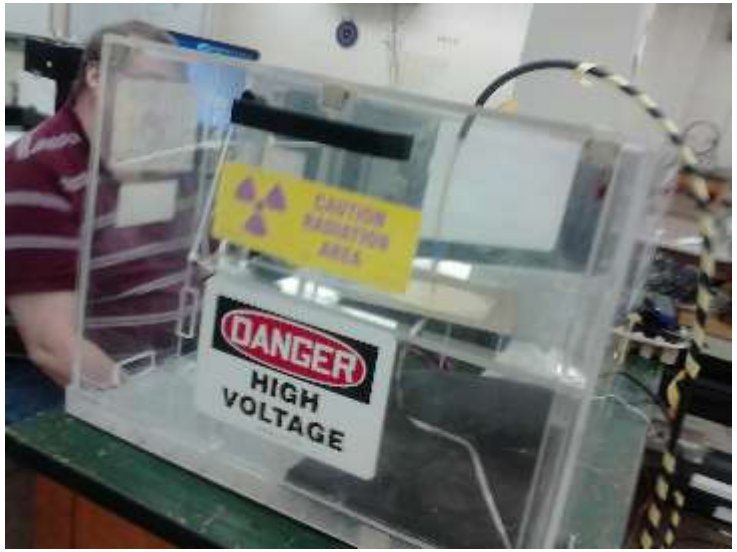

Went immediately to 40 kV!
Switched to 80 kV Power Supply
Sparks “around” the piece at 65 kV
(NOT the limit for closed geometry)

- 32 kV (round to 40 kV) is operating point.
- Likely 1 mm thickness is enough for sPHENIX.
- Since 1 mm is only 0.35% of radiation length solution will work.
- The question becomes exactly how we build this field cage.

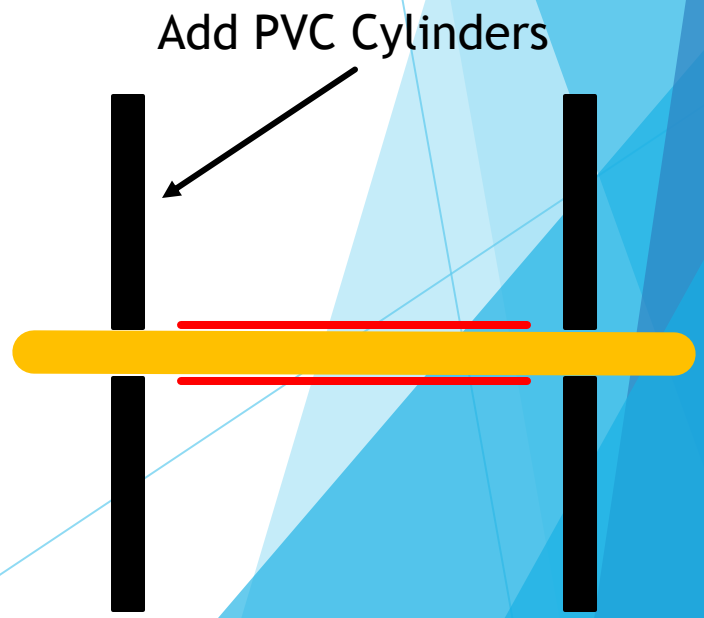

HV Testing…

Reminder: Operates at 32 kV + GEM voltage, ~35 kV.

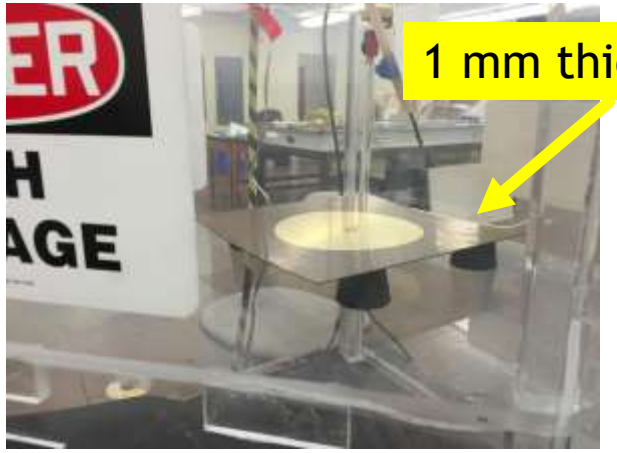

Sparks around edge, through air.

Add PVC pipe to lengthen air path…

- My next biggest HV power supply is 450 kV, but that one powers injector to SBU tandem accelerator.
- Rich Lefferts believes that when this one sparks through material, that (like the 20 kV, 40 kV, and 80 kV units) it will not hurt the power supply.
- We'll likely run that test in the coming week.

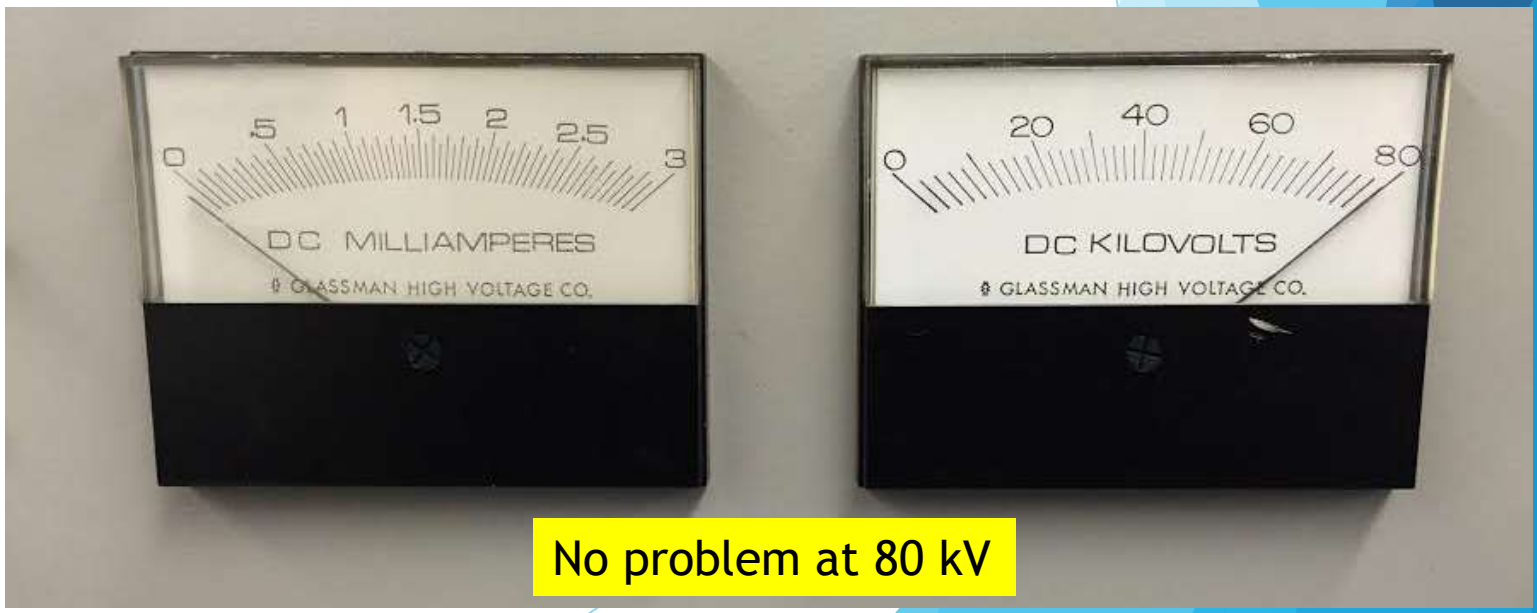

Mandrel

Mandrel & Tooling similar to Lathe…

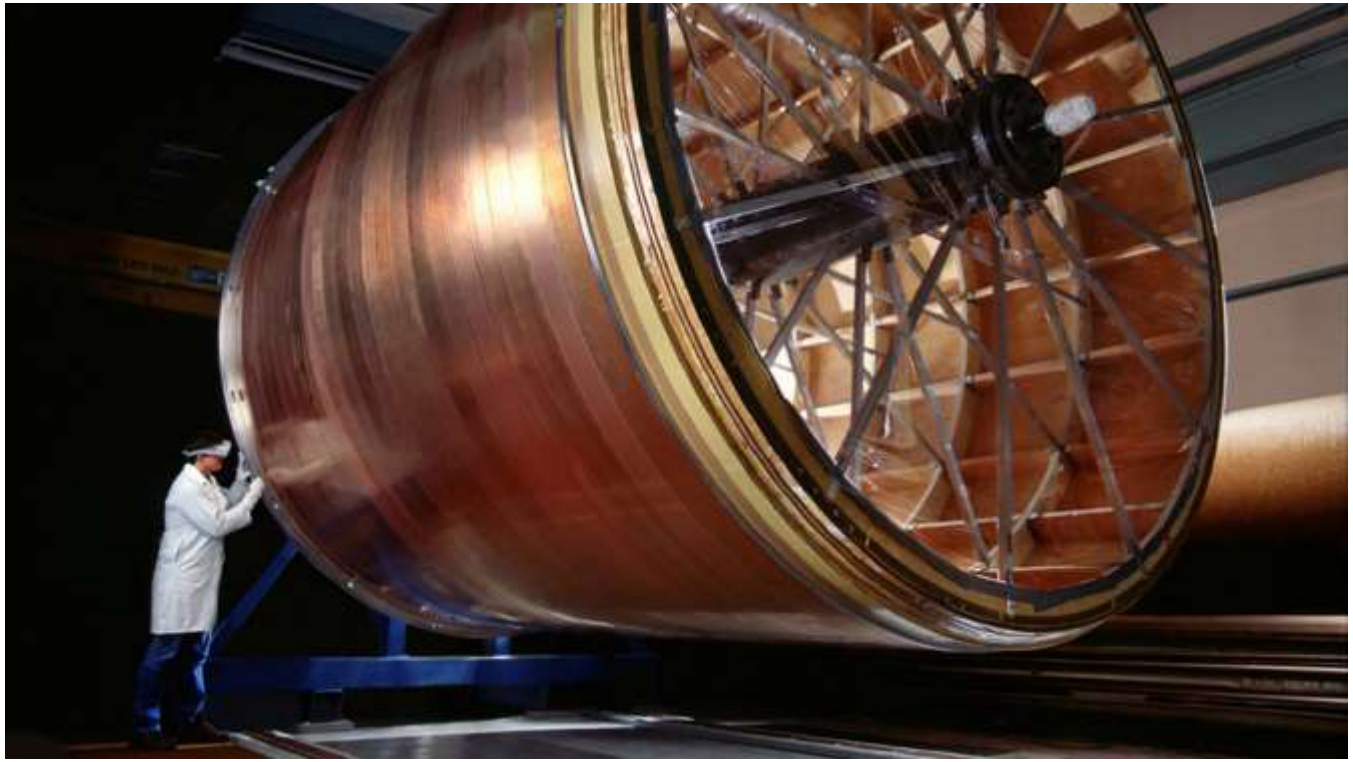

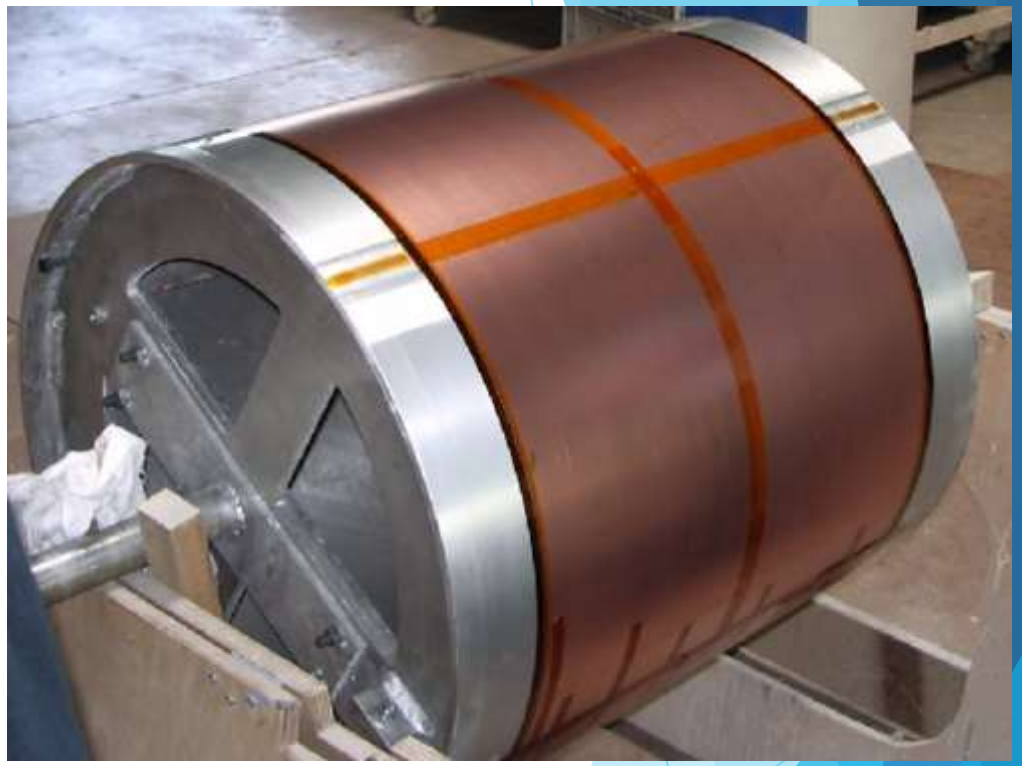

- Hexcell honeycomb sandwiches are familiar to many in planar form.
- To do the same in a cylinder, you need a “Mandrel”.
- Question: How do you get the damned thing off the mandrel?

Field Cage Construction

Niv Ramasubramanian: SBU physics grad student, BA in engineering.

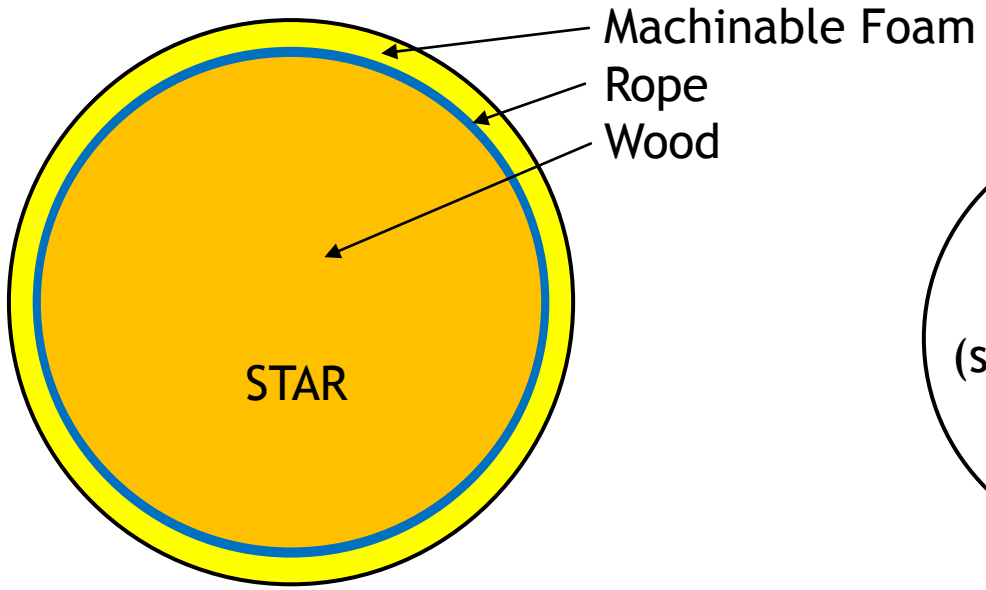

- Wooden cylinder.
- Double layer of rope on cylinder.
- Machinable foam:
  - Turned (like a lathe) to correct outer radius.
- After layers glued…rope pulled from end to free the field cage.

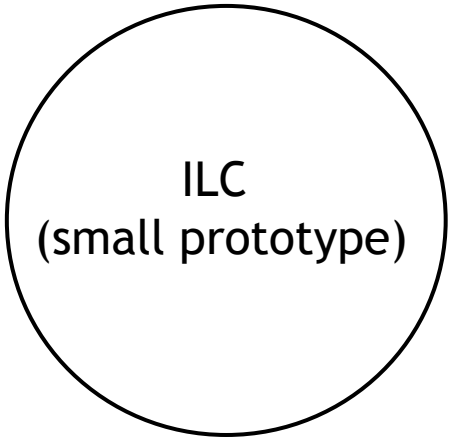

- Steel cylinder with internal mechanics.
- Internal mechanics allows the cylinder to retract from the field cage at the end.

sPHENIX

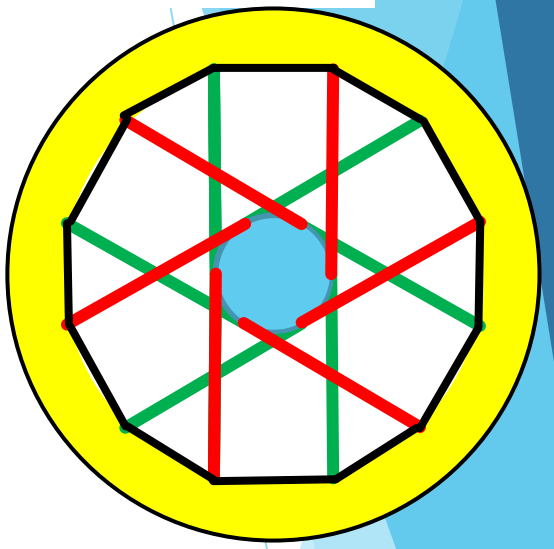

- Compromise between STAR and ILC
- The cylinder supporting the machinable foam is like a bicycle wheel (sturdy)
- 3 Wheels make a cylinder.
- Since ½ length is only 80cm, we can reach in to disassemble 80-20 pieces freeing the field cage.

Design progress

3D CAD using AutoDesk Inventor Pro
FREE to students and faculty.
Same software used by Rich Ruggiero

- Last time we agreed:
  - R_{outer}=80 cm is too big.
  - R_{outer} should be somewhere in the range of 76-78 cm.
- Calculations show that if we design our mandrel to 77cm, we can support either 78 or 76 cm by choosing to cut more or less from our 2” thick foam block.
- On the right is the wheel assembly in 3D CAD.

- The central “hub” will be cut from Aluminum plate in the SBU shops.
- The spokes are 1.5” 8020 extruded material.
- Three “wheels” make up the inner cage of the mandrel.

NOTE: Last night (2/25/2016), the engineering group selected 78 cm as the TPC outer radius:
10 cm for upgrade plus 1 cm stay clear to each side.

Mandrel CAD Design.

- Each wheel is held to the precision steel shaft via a collar.
- The collar is positioned by the SBU shop to be centered in the wheel.
- The foam blocks are held from the inside via screws (e.g. drywall screws).
- “Even” numbered blocks: square sides.
- “Odd” numbered blocks angled sides.
- Because of the asymmetry, there is a lip at every edge that will be removed.

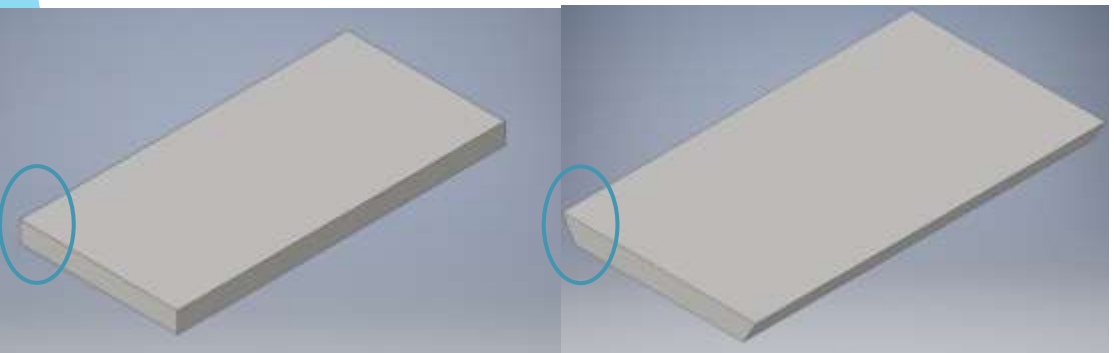

Samples of 3 densities of foam in hand & “butterboard”
Currently favoring the highest density rohacell

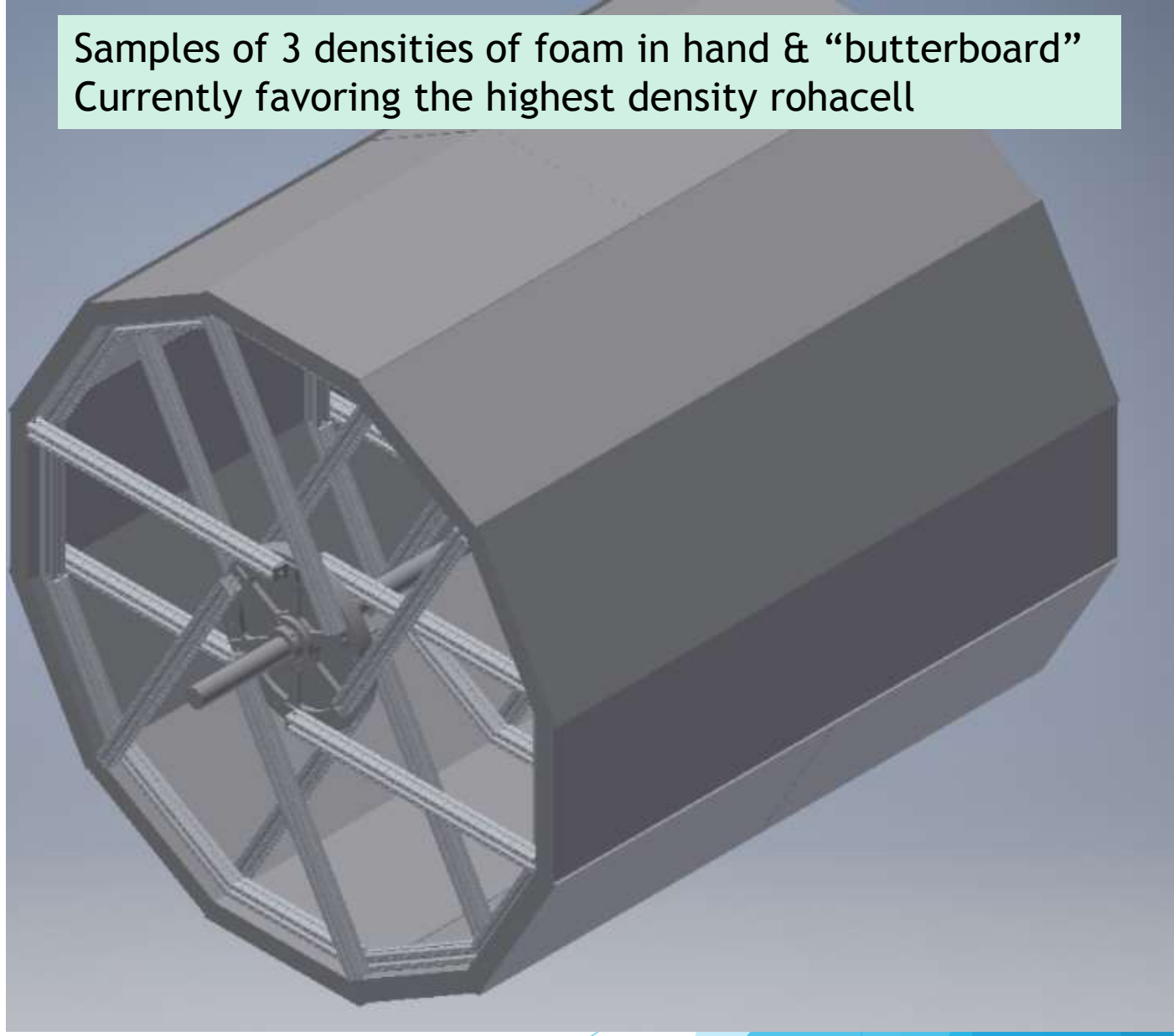

Reminder: Basic concept is to turn (as in lathe) the rohacell foam into a precise cylinder to lay up the field cage walls.

Mandrel in real life

End Cap Design

- The End Cap design requires significantly more work!
- This is the “interface” to the rest of sPHENIX and must be designed collaboratively with BNL engineering.
  - Flatness critical for field shaping.
  - Low deflection required.
- Nonetheless, we should spend some time on the conceptual foundation of what we want:
  - STAR/ALICE = MASSIVE WHEELS.
    - Followed by flux return (STAR) or muon measurement (ALICE).
  - ILC follows the end caps with additional detector layers.
    - Must be thin to make good measurements behind it.

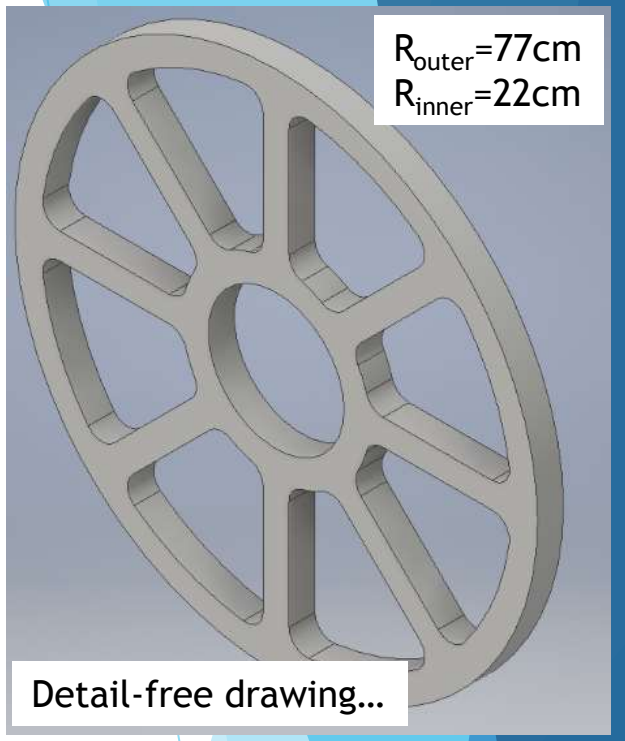

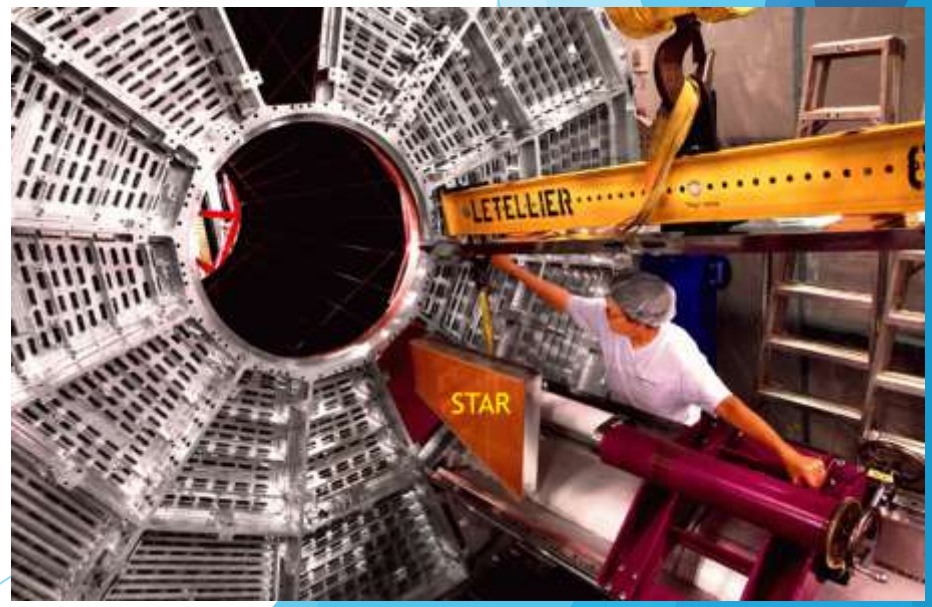

ILD @ ILC

- STAR-like diameter
- ALICE-like length

- Goal: σ~100-150 μm
- Test: σ = 120 μm

Work at Cornell: development of the endplate and module mechanical structure to satisfy the material and rigidity requirements of the ILD.

The ILD TPC has dimensions:
outer radius 1808 mm
inner radius 329 mm
half length 2350 mm

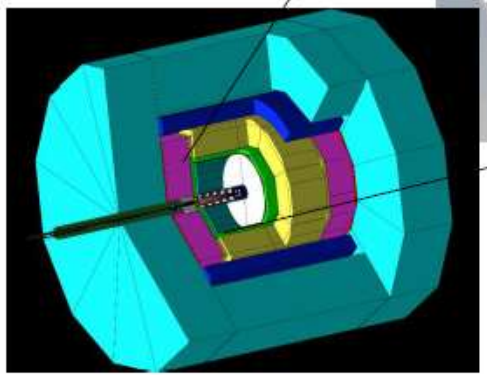

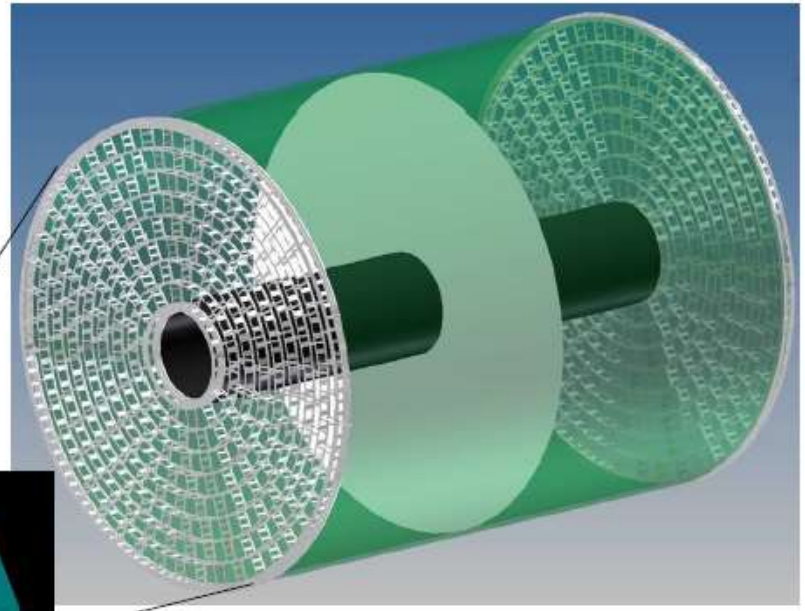

→ Prototype tests during development of the ILD TPC endplate design
→ ILD TPC endplate design, analysis
→ LP2 endplate construction and testing as a validation of the ILD design
→ Further measurements on the LP2 endplate
→ Further analysis on the ILD endplate design
→ Comments on viability of constructing the ILD endplate

Evolution

- Two are thin enough:
  - Hybrid
  - Space Frame
- ILD finds that the Hybrid is not rigid enough under pressure.
- Our small size could result in a different solution.

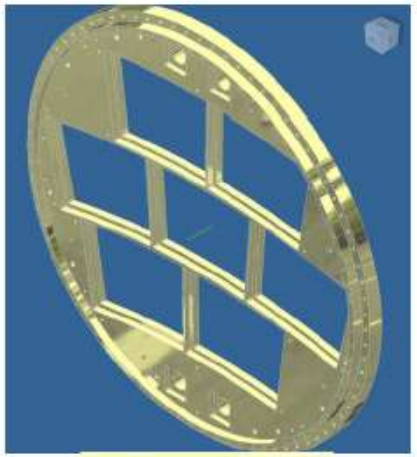

LP1 endplate, thick aluminum

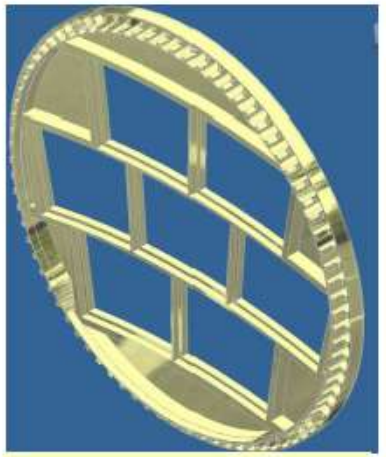

lightened, all aluminum

aluminum/ carbon fiber hybrid

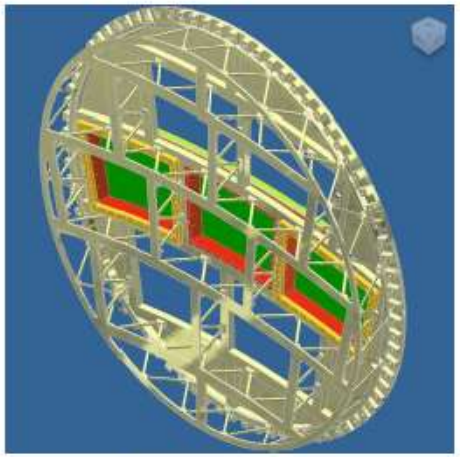

space frame

Various technologies were considered for the ILD endplate
(illustrated here for an LP1-size endplate).

The LP1 endplate structure is rejected because of high material.

Various **lighted endplates** illustrated contributions to the endplate strength.

Low material **hybrid construction** was considered in an effort
to provide the strength of the LP1 design, with significantly reduced material.
But, there is insufficient rigidity when scaled to the size of the ILD.

Only a **space-frame** promises to provide the required strength-to-material.

Tough Beans…

- Real life is always tougher than simulation…
- Still not bad at all.
- ILD is headed toward space frame, but it is not clear that this is the right choice for us…

Validation of the FEA with 0.8 meter diameter LP2 endplate

The FEA predicts a longitudinal deflection of 23 microns / 100 N load.

(with the load applied at the center module.)

Measured deflection is 27 microns/100 N load, 17% higher.

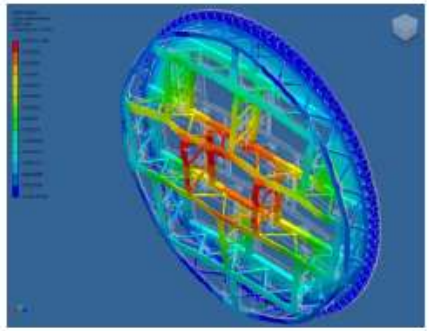

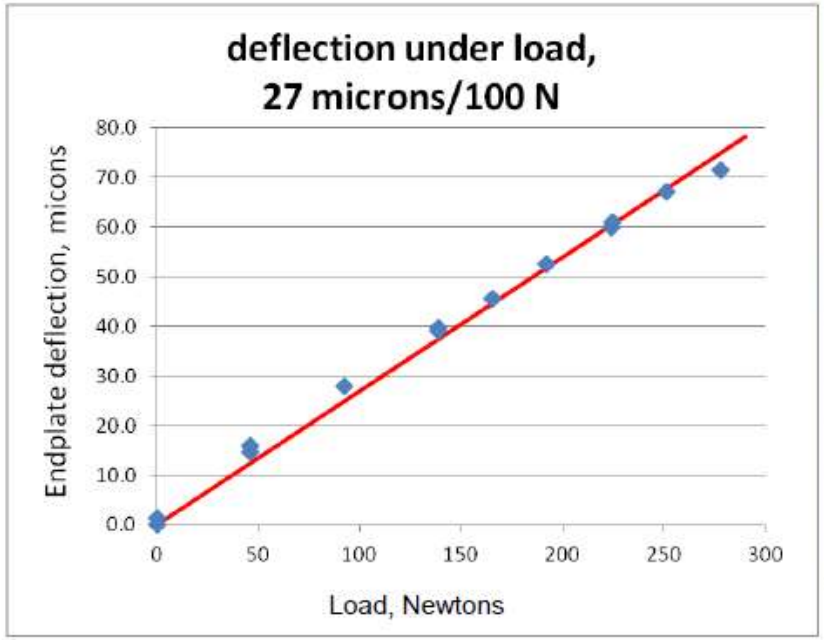

measuring the deflection

Comparison

- Because of mechanical size considerations, sPHENIX will have a MUCH easier time meeting deflection specs.
- Simpler to build designs are actually thinner than the space frame!
- The concept of going with small modules is also quite a change.

Comparison of deflection for LP1/LP2 endplates: FEA vs. measurements

	mass kg	material %X_0	calculated deflection µm (100 N)	stress MPa (yield: 241)	measured deflection µm (100 N)
LP1	**18.87**	**16.9**	**29**	**1.5**	**33**
LP2 Space-Frame (strut or equivalent plate)	**8.38**	**7.5**	**23**	**4.2**	**27**
Lightened	8.93	8.0	68	3.2	
Al-C hybrid (channeled plus fiber)	**Al 7.35 C 1.29**	**7.2**	**(68-168)**	**(3.2-4.8)**	
Channeled	Al 7.35	6.5	168	4.8	

The original LP1 endplate was compared to the FEA earlier.

In both LP1 and LP2, the measured deflection is about 15% higher than from the FEA, which is close for the level of detail of the model.

Summary

- Large experienced team.
- Methods to minimize space charge troubles via relaxing dE/dx requirements.
- Detector usable into EIC era.
- Prototype stage field cage designed to be re-used for real detector.
- DoE project would focus on the avalanche stage and electronics (possibly STAR iTPC).